Regional Networks Underlying Interhemispheric Connectivity: An EEG and DTI Study in Healthy Ageing and Amnestic Mild Cognitive Impairment

Stefan J. Teipel,[1,2*] Oliver Pogarell,[1] Thomas Meindl,[3] Olaf Dietrich,[3] Djyldyz Sydykova,[1] Ulrike Hunklinger,[1] Bea Georgii,[1] Christoph Mulert,[1] Maximilian F. Reiser,[3] Hans-Jürgen Möller,[1] and Harald Hampel[1,4]

[1]*Department of Psychiatry, University of Rostock, Rostock, Germany*
[2]*Department of Psychiatry, Dementia and Neuroimaging Section, Alzheimer Memorial Center, Ludwig-Maximilian University, Munich, Germany*
[3]*Department of Clinical Radiology, University Hospitals—Grosshadern, Ludwig-Maximilian University, Munich, Germany*
[4]*Discipline of Psychiatry, School of Medicine and Trinity College Institute of Neuroscience (TCIN), Trinity College Dublin, The Adelaide and Meath Hospital incorporating the National Children's Hospital (AMiNCH), Dublin, Ireland*

Abstract: Interhemispheric coherence derived from electroencephalogram (EEG) recordings is a measure of functional interhemispheric connectivity. Diffusion tensor imaging (DTI) determines the integrity of subcortical fiber tracts. We studied the pattern of subcortical fiber tracts underlying interhemispheric coherence and its alteration in 16 subjects with amnestic mild cognitive impairment (MCI), an at risk syndrome for Alzheimer's disease, and 20 cognitively healthy elderly control subjects using resting state EEG and high resolution DTI at 3 T. We used a multivariate network approach based on principal component analysis to determine effects of coherence on the regional pattern of diffusivity. Temporo-parietal coherence in the α band was significantly correlated with diffusivity in predominantly posterior white matter tracts including posterior corpus callosum, parietal, temporal and occipital lobe white matter, thalamus, midbrain, pons, and cerebellum, both in MCI subjects and controls ($P < 0.05$). In MCI subjects, frontal coherence in the α band was significantly correlated with a predominately frontal pattern of diffusivity including fiber tracts of the anterior corpus callosum, frontal lobe white matter, thalamus, pons, and cerebellum ($P < 0.05$). The study provides a methodology to access specific networks of subcortical fiber tracts subserving the maintenance of interhemispheric resting state coherence in the human brain. *Hum Brain Mapp 30:2098–2119, 2009.* **© 2008 Wiley-Liss, Inc.**

Key words: cortical connectivity; interhemispheric coherence; diffusion tensor imaging; Alzheimer's disease; neuronal networks

Contract grant sponsors: Medical Faculty of the Ludwig-Maximilian University (Munich, Germany), Hirnliga e. V. (Nürmbrecht, Germany), Janssen-CILAG (Neuss, Germany); Contract grant sponsor: Bundesministerium für Bildung und Forschung; Contract grant number: BMBF 01 GI 0102.

*Correspondence to: Stefan J. Teipel, Department of Psychiatry and Psychotherapy, University of Rostock, Gehlsheimer Str. 20, 18147 Rostock, Germany. E-mail: stefan.teipel@med.uni-rostock.de

Received for publication 15 February 2008; Revised 10 July 2008; Accepted 15 July 2008

DOI: 10.1002/hbm.20652

Published online 9 September 2008 in Wiley InterScience (www.interscience.wiley.com).

INTRODUCTION

The human brain is organized in segregated functional networks that require intact intracortical connectivity [Sporns et al., 2004]. Interhemispheric coherence derived from electroencephalogram (EEG) is a sensitive marker of functional interhemispheric connectivity in the human brain [Walter, 1968]. Functional connectivity is based on the integrity of neuronal fibers crossing through the cerebral white matter. Diffusion tensor imaging (DTI) is a recently established imaging modality to determine the microstructural integrity of subcortical fiber tracts in the living human brain. DTI is based on the random movement of water molecules that is spatially restricted in highly organized media such as the cerebral white matter. Fractional anisotropy (FA) as a marker of movement directionality and mean diffusivity (MD) as an indicator of overall diffusivity are scalar parameters derived from DTI acquisitions and serve as sensitive measures for the integrity of cerebral fiber tracts [Beaulieu, 2002].

Alzheimer's disease (AD) is the most frequent neurodegenerative disorder in humans. It selectively involves cerebral neuronal networks subserving higher cognitive functions [Morrison et al., 1986]. Thus, AD is a paradigm for the disruption of regional cortical connectivity, and its functional and behavioral consequences in humans [Delbeuck et al., 2003]. Very early changes of cortical disconnection associated with AD can be studied in clinical at risk groups for AD, in particular in subjects with amnestic mild cognitive impairment (MCI). These patients have predominant memory impairment without decline of general cognitive function [Petersen et al., 2001]. Subjects with MCI have an increased risk to develop AD during clinical follow up with a conversion rate between 20 and 40% per year [Busse et al., 2006; Devanand et al., 1997; Maioli et al., 2007; Petersen et al., 1999].

A large range of studies has investigated interhemispheric coherence in AD and MCI. Using EEG, interhemispheric coherence has been consistently found reduced in AD patients [Jelic et al., 2000; Pogarell et al., 2005; Prichep, 2007; Tao and Tian, 2005], in agreement with evidence from neuropathological studies indicating selective involvement of intracortical projecting neurons in cortical layers III and V [Giannakopoulos et al., 1997; Pearson et al. 1985]. Reduction of interhemispheric coherence is in line with functional imaging studies as well using PET or fMRI, demonstrating reduced coupling between widespread areas of association cortex in AD [Backman et al., 2000; Bokde et al., 2006; Bookheimer et al., 2000; Delbeuck et al., 2003; Greicius et al., 2004; Hampel et al., 2002]. In contrast, resting state interhemispheric coherence was not different between MCI and controls in several studies [Jelic et al., 1996, 2000; Jiang and Zheng, 2006; Tao and Tian, 2005]. However, intrahemispheric fronto-parietal coherence differs between MCI patients and controls [Babiloni et al., 2006] and predicts conversion into AD in MCI patients [Rossini et al., 2006]. Additionally, high dimensional features of EEG signal as detected by artificial neuronal networks [Rossini et al., 2008] and global EEG synchronization discriminate between MCI patients and controls [Koenig et al., 2005; Prichep, 2007].

Consistent with a decline of cortical connectivity and impairment of axonal and dendritic integrity [Brun and Englund, 1986; Kowall and Kosik, 1987; Leys et al., 1991; Su et al., 1993] early in the disease process of AD, studies using DTI found decline of FA as marker of fiber loss in posterior corpus callosum, fasciculus longitudinalis superior, temporal lobe, and cingulate white matter [Bozzali et al., 2002; Fellgiebel et al., 2004, 2005; Head et al., 2004; Müller et al., 2005; Naggara et al., 2006; Rose et al., 2000; Stahl et al., 2007; Takahashi et al., 2002; Yoshiura et al., 2002]. One study using voxel-based analysis of low-dimensionally normalized FA maps found significant reductions of FA in posterior white matter areas [Medina et al., 2006]. However, low-dimensional normalization, as employed in this study, is not able to separate reductions of FA from effects of atrophy. Employing multivariate analysis of high-dimensionally normalized FA maps, we had found significant decline of FA in intracortical projecting fiber tracts in AD patients compared with controls [Teipel et al., 2007]. This method accounted for effects of atrophy and by using multivariate analysis based on principal component analysis uncovered the entire network of fiber tract changes in AD. In MCI, several studies showed significant reductions of markers of fiber tract integrity in subcortical white matter, including the posterior cingulated [Fellgiebel et al., 2005; Zhang et al., 2007], hippocampus [Fellgiebel et al., 2006; Muller et al., 2007], and posterior white matter [Fellgiebel et al., 2004; Huang and Auchus, 2007]; [Medina et al., 2006; Rose et al., 2006].

In this study, we investigated whether regional interhemispheric coherence determined using resting state EEG was associated with distributed networks of subcortical fiber tracts both in healthy aging and in amnestic MCI. We expected to uncover specific networks of white matter tracts including corpus callosum, thalamus, and brainstem that subserve the maintenance of frontal and posterior interhemispheric coherence. Following the assumption that amnestic MCI represents an early clinical predementia stage of AD, we further expected that the effects would be more pronounced in MCI subjects than in controls. AD pathology affecting intracortical connectivity would lead to both, impairment of intracortical projecting fiber tracts and interhemispheric coherence. Correlations between the degree of functional integrity (measured through interhemispheric coherence) and fiber degeneration (measured through regional diffusivity) would be stronger if functional integrity and fiber tract integrity would be influenced in the same direction through the effect of AD pathology. We used high-dimensional normalization to account for effects of atrophy on FA and MD values and employed multivariate analysis to reveal the entire network of fiber tracts underlying interhemispheric coherence. As we acquired DTI at 3 T to improve signal to noise ratio

and spatial resolution, we met higher distortion artifacts. Therefore, we used parallel imaging that permits a reduction of echo times without loss of spatial resolution to reduce distortion artifacts [Stahl et al., 2007].

SUBJECTS AND METHODS

Subjects

We examined 16 subjects with amnestic MCI (mean age: 73.6 (SD 7.8) years, ranging from 60 to 88 years, 7 women) and 20 healthy elderly subjects [mean age: 67.0 (SD 7.3) years, ranging from 56 to 83 years, 9 women]. The MCI and control groups differed significantly in age (*t*-test: $P = 0.014$, $T = -2.598$, and 34 degrees of freedom), but showed a similar gender distribution ($\chi^2 = 0.006$, 1 degree of freedom, and $P = 0.94$). The Mini-Mental-Status Examination (MMSE) was used to assess the degree of overall cognitive impairment [Folstein et al., 1975]. Groups differed significantly in MMSE scores, with 26.5 (SD 1.1) points in MCI and 29.0 (SD 0.7) points in control subjects ($P < 0.001$, Mann–Whitney $U = 6.0$).

Amnestic MCI was diagnosed according to Mayo Criteria [Petersen, 2004] with subjects showing subjective memory impairment, scoring more than 1.5 standard deviations below the age- and education-adjusted mean in tests of immediate and delayed verbal and non verbal memory, having unimpaired general cognition and activities of daily living and receiving a CDR rating of 0.5 [Fillenbaum et al., 1996]. Healthy volunteers were generally spouses of our patients, who had no subjective memory complaints and scored within one standard deviation of the mean of all subtests of the CERAD cognitive battery [Berres et al., 2000] and the trail making test part A and B [Chen et al., 2000], and received a Shulman score of 1 in the clock drawing test [Shulman et al., 1986]. All healthy control subjects scored 0 in the CDR rating [Fillenbaum et al., 1996].

The clinical assessment included detailed medical history, clinical, psychiatric, neurological, and neuropsychological examinations (CERAD battery [Berres et al., 2000], Clock-drawing-test [Shulman et al., 1986], and trail-making test [Chen et al., 2000]), and laboratory tests (complete blood count, electrolytes, glucose, blood urea nitrogen, creatinine, liver-associated enzymes, cholesterol, HDL, triglycerides, serum B12, folate, thyroid function tests, coagulation, and serum iron).

Selection of subjects included a semiquantitative rating of T2-weighted MRI scans [Scheltens et al., 1993]. Only those subjects were included, who had no subcortical white matter hyperintensities exceeding 10 mm in diameter or 3 in number.

All patients and controls were only examined when they gave their written consent. The study was approved by the institutional review board of the Medical Faculty of the University of Munich.

MRI Acquisition

MRI acquisitions of the brain were conducted with a 3.0 T scanner with parallel imaging capabilities (Magnetom TRIO, Siemens, Erlangen, Germany), maximum gradient strength: 45 mT/m, maximum slew rate: 200 T/m/s, 12 element head coil.

Subjects were scanned in a single session without changing their position in the scanner. The following sequences were used: for anatomical reference, a sagittal high-resolution three-dimensional gradient-echo sequence was performed (magnetization prepared rapid gradient echo MPRAGE, field-of-view 250 mm, spatial resolution $0.8 \times 0.8 \times 0.8$ mm^3, repetition time 14 ms, echo time 7.61 ms, flip angle 20°, number of slices 160). To identify white matter lesions a two-dimensional T2-weighted sequence was performed (fluid attenuation inversion recovery FLAIR, field-of-view 230 mm, repetition time 9,000 ms, echo time 117 ms, voxel size $0.9 \times 0.9 \times 5.0$ mm^3, TA 3:20 min, flip angle 180, number of slices 28, acceleration factor 2).

Diffusion-weighted imaging was performed with an echo-planar-imaging sequence. (field-of-view 256 mm, repetition time 9,300 ms, echo time 102 ms, voxel size $2.0 \times 2.0 \times 2.0$ mm^3, four-repeated acquisitions, *b*-value 1 = 0, *b*-value 2 = 1,000, 12 directions, noise level 10, slice thickness 2.0 mm, 64 slices, no overlap).

EEG Recording

EEG recordings were performed in a sound-attenuated, electrically shielded room. Patients were seated in a reclining chair, 32 electrodes were placed on the scalp using electrocaps (AFZ, FZ, CZ, PZ, FP1/2, F3/4, F7/8, FC1/2, FC5/6, C3/4, CP6/7, T1/2, T3/4, T5/6, P3/4, P9/10, O1/2) and at A1/2 according to the extended international 10–20 system plus T1/2 [Nuwer et al., 1998; Silverman, 1960]. Additional electrodes above the left eye and at the left ocular canthis were used to simultaneously record the electrooculogram.

Impedances of all electrodes were kept below 5 kΩ throughout the session. Electric activity was recorded for 600 s in a wakeful resting condition with eyes closed, using a computerized acquisition system (Neuroscan Synamps®, bandpass 0.16–70 Hz, sample rate of 1,000 Hz) with Cz as reference.

DTI Data Processing

Preprocessing

DTI data were preprocessed using the DTI toolbox of the FSL software (http://www.fmrib.ox.ac.uk/fsl/written mainly by members of the Analysis Group, FMRIB, Oxford, UK. Version 3.2). Susceptibility artifacts were corrected using maximization of mutual information to estimate the three parameters of a geometric distortion model inferred from the acquisition principle [Mangin et al., 2002]. From the 12 gradient directions we derived a

12 × 12-tensor to extract eigenvalues and eigenvectors to determine FA and MD maps from the gradient scans [Teipel et al., 2007].

The analysis method was implemented within Matlab 6.5 (MathWorks, Natwick, MA) through Statistical Parametric Mapping [Friston et al., 1995a, 1995b] (SPM 2, Wellcome Department of Imaging Neuroscience, London; available at http://www.fil.ion.ucl.ac.uk/spm). The MRI scans were processed in three subsequent steps that have previously been described in detail [Teipel et al., 2007].

Normalization of 3D sequence and groups specific template

Each anatomical scan was normalized to the standard MNI T1 MRI template using a low dimensional algorithm with a set of nonlinear basis functions [Ashburner and Friston, 2000; Ashburner et al., 1997]. The normalized anatomical scans were smoothed (12-mm full width at half maximum isotropic Gaussian kernel) and averaged across all subjects to obtain an anatomical average image. One good quality MRI scan of a healthy control subject then was normalized to this anatomical average image using high-dimensional normalization with symmetric priors [Ashburner et al., 1999] resulting in a pretemplate image. Finally, the MRI scan in native space of the same subject was normalized to this pretemplate image using high-dimensional normalization. The resulting volume in standard space served as an anatomical template for subsequent normalizations. The template MRI was segmented into CSF, gray matter, and white matter compartments using the SPM2 prior probability maps. The SPM segmentation employs a mixture model cluster analysis (after correcting for nonuniformity in image intensity) to identify voxel intensities that match particular tissue types combined with a priori probabilistic knowledge of the spatial distribution of tissues derived from gray and white matter and CSF prior probability images (priors) [Ashburner and Friston, 1997].

High-dimensional normalization of anatomical scans to standard template

The individual anatomical scans in standard space (after low-dimensional normalization) were normalized to the anatomical template using high-dimensional image warping with symmetric priors. These normalized images were resliced to a final voxel size of 1.0 mm^3.

Normalization of FA and MD maps

The low- and high-dimensional normalization parameters of the preceding steps were sequentially applied to the spatially coregistered FA and MD maps, resulting in FA and MD maps projected into standard space. After the normalization procedure, morphological differences of anatomical and FA and MD maps between subjects were minimized on a local scale.

Coherence Analysis

Analyses were performed off line in Brain Vision Analyzer® software (v 0.94c, Brain Products, Munich, Germany). EEG recordings were visually assessed and controlled for artifacts (eye movements, blinks, muscle activity) subsequently by two raters. Because coherence is influenced by the subjects' vigilance or alertness [Barry et al., 2004; Leocani et al., 2000], EEG epochs indicating somnolence or reduced alertness, defined by the presence of less than 50% occipital background activity in a stepwise visual screening per 2-s epochs, were further excluded. Artifact-free, alertness-controlled data were rereferenced to linked ears and segmented into 2-s epochs. At least 30 2-s segments were required from each subject for fast Fourier transformation (FFT) and power spectral analysis. Power spectra were calculated for δ (1–3 Hz), θ (4–7 Hz), α (8–12 Hz), and β (13–32 Hz) frequency bands. Subsequently interhemispheric coherences were computed for each of the frequency bands between the following channels: F3-F4, F7-F8, C3-C4, T3-T4, T5-T6, P3-P4, and O1-O2.

Coherence is a function of power spectral outputs for the two pairs of electrodes with values between 0 and 1 at a given frequency. A coherence value of 0 indicates a random association between the signals (phases are dispersed); a value of 1 means that the correlated signals are phase locked, indicating shared activity of the channels. Thus coherence is a quantitative measure of the similarity of signals in a given frequency band [Pogarell et al., 2005]. EEG-recordings were performed referenced to Cz electrode. For quantitative analyses (qEEG, coherence analyses), our data were rereferenced to the linked ears offline before they were transformed any further. Regarding the reference for coherence analyses our choice (linked ears) was based on considerations taking into account the literature, coherence data from other groups, and our own experience [Babiloni et al., 1995; Barry et al., 2004, 2005, 2006; Nunez et al., 1999, 1997; Pogarell et al., 2005; Thatcher, 1992; Thatcher et al. 1986, 2007]. This approach is in line with other groups (e.g. [Barry et al., 2004, 2005, 2006; Thatcher, 1992; Thatcher et al., 1986, 2007]) who also used linked-ears reference and have discussed this issue extensively (e.g. [Barry et al., 2004]). Linked ears reference might display a problem of potential overestimation of coherence values. This effect, however, is increasingly reduced for longer distances between electrodes and reference, which is the case in our study. Also much care was taken to balance the impedances between the ear electrodes and to comprehensively reject any artifacts manually and off line before analyzing the data any further.

Data were compiled into three groups: frontal (Fx), temporo-parietal (Tx, Px, Cx), and occipital (Ox). This method of reducing data has also been applied in other studies [Barry et al., 2004, 2005]. Because we used resting state EEG, devoid of artifacts, the EEG was biased for the presence of regular background activity, comprising α (and β) activities, which were included in our analyses accord-

ingly. For statistical analysis we only considered the frontal and temporo-parietal coherence, as we expected the largest effects of AD pathology on these regions.

Statistical Analysis

Prior to principal component analysis, voxels from outside the white matter were removed from the spatially normalized FA and MD maps by means of a mask derived from the white matter map of the template brain. The masked FA and MD maps were smoothed with a 12-mm FWHM Gaussian kernel. Images were scaled to the same mean value and standard deviation using a voxelwise *z*-transformation:

$$z_{i,k} = \frac{x_{i,k} - \bar{x}_k}{s_k}$$

where $x_{i,k}$ is the FA/MD value of voxel i in scan k, $\bar{x}_k$ is mean value across all x_i of scan k and s is the standard-deviation across all x_i of scan k.

The multivariate approach that was employed in this study has been adapted for DTI data based on the paper by [Friston et al., 1996] in an earlier study [Teipel et al., 2007]. We followed three subsequent steps that will only briefly be described in the following section. For further details we refer to [Teipel et al., 2007] and [Friston et al., 1996]

First, the high-dimensionally normalized FA and MD maps were subjected to principal component analysis within the MCI and control groups. Thus, the dimensionality of the data was reduced to 16 components in the MCI and 20 principal components in the control group. The first 10–12 principal components accounted for about 2/3 of the variance in the FA and MD maps, respectively. In the terminology of linear algebra the principal components are the eigenvectors of the ($n \times p$) data matrix X, where n is the number of scans (observations) and p is the number of voxels (variables). In the terminology of image analysis, the eigenvectors are called the eigenimages.

Second, we determined the significance of the hypothesized effect of coherence on FA and MD values using multivariate analysis of variance (MANCOVA). We employed two linear models within each group (MCI and controls) with anterior and posterior interhemispheric coherence, respectively, as independent variables and the principal components from the FA and MD maps, respectively, as multivariate dependent variables.

Third, we characterized the spatial distribution of these effects using canonical variate analysis in terms of the canonical vector that best captured the effect of diagnosis. To characterize the effect in terms of its spatial topography, we aimed to find a linear combination of the principal components that best express the group effects when compared with error effects. To this end, we defined canonical images in the observation space such that the variance ratio between the effect of interest, and the total error sum of squares was maximized. The canonical images in voxel space were then found by rotating the canonical images in observation space into voxel space with the original matrix of principal components, termed matrix C. The matrix C now contained the voxel values of the canonical images. Each column of C has an associated canonical value that serves to estimate whether a particular canonical image is important. As the canonical value corresponds to a variance ratio it can be compared to an F distribution with denominator degrees of freedom equal to the rank of the design matrix and nominator degrees of freedom equal to the number of scans minus the rank of the design matrix (= degrees of freedom of the error term). We considered a canonical image important if its canonical value exceeded the critical F threshold for $P < 0.05$.

The multivariate approach is independent from assumptions about spatial correlations and from adjustments for multiple comparisons. One has, however, to note that this model makes inferences about all the voxels of a multivariate variable (eigenvector), not a particular voxel or set of voxels.

Calculations were carried out using an algorithm written in MATLAB v. 5.3 (Mathworks, Newton, MA).

Identification of Voxel With Peak Loading

The 98th percentile was used as threshold for voxel with highest positive or negative loading on the canonical image. The Talairach–Tournoux coordinates of these voxel were determined using in-house software written in C. The program produces a listing of all local maxima and minima (above or below a given threshold) of the canonical image with each local peak at least 1 cm away from neighboring peaks.

RESULTS

Effects of Diagnosis on Coherence

Temporo-parietal coherence in the α band was significantly reduced in MCI patients compared with controls after controlling for age in a linear model ($F_2^{33} = 10.3$, $P < 0.003$). There were no significant differences between groups in any other frontal or posterior α and β bands (Table I).

FA Maps

MCI patients

Temporo-parietal α coherence. Applying PCA we found seven eigenimages with eigenvalues greater than unity. We assessed the significance of the effect of coherence with a design matrix having 16 rows (one for each scan) and two columns, one for the mean effect and one for the effect of temporo-parietal coherence, respectively. The data were reduced to the first seven eigenvectors having eigen-

TABLE I. α- and β-coherence in MCI patients and controls

	Frontal coherence		Temporo-parietal coherence	
Diagnosis	α	β	α[a]	β
Controls	0.25 (0.11)	0.09 (0.05)	0.08 (0.03)	0.03 (0.02)
MCI	0.21 (0.08)	0.11 (0.10)	0.05 (0.02)	0.04 (0.06)

Coherences were averaged for the α and β bands across several electrode positions (for details see text).
[a] Significantly different between MCI patients and controls after controlling for age ($F_2^{33} = 10.3$, $P < 0.003$).

values greater than unity. The resulting matrix was subject to MANCOVA. Wilk's lambda after transformation corresponded to $\chi^2 = 33.68$ with 14 degrees of freedom, $P < 0.005$. The effect of coherence was almost completely accounted for by the second canonical image. Its canonical value was 143 and larger than the threshold $F_2^{14} = 99.4$ for $P < 0.01$. We divided the canonical image in one image containing only voxels with high positive loadings (positive components) and one image containing only voxels with high negative loadings (negative components) on the canonical image. Subsequently, we considered only the negative components representing a decline of FA associated with a decline in coherence. Figure 1 shows the negative components of the second canonical image projected onto the T1-weighted MRI template in standard space. The 80th percentile threshold was used to show only the most relevant features. Table II shows the Talairach-Tournoux coordinates of the voxel with the highest negative loadings on the canonical image lying above the 95th percentile.

Voxels with high negative loadings, i.e. relatively smaller FA values with reduced coherence, were located predominantly in posterior white matter areas, including posterior corpus callosum, temporal, parietal and occipital lobe white matter, parahippocampal gyrus white matter, internal capsule, and white matter areas in proximity to thalamic nuclei. Additionally infratentorial white matter areas were involved including cerebellum, midbrain (pedunculi cerebri), and pons.

Frontal α coherence. For the effect of frontal coherence we found seven eigenvectors having eigenvalues greater than unity. From MANOVA, Wilk's lambda after transformation corresponded to $\chi^2 = 31.74$ with 14 degrees of freedom, $P < 0.005$. The effect of coherence was almost completely accounted for by the second canonical image. Its canonical value was 118.4 and larger than the threshold $F_2^{14} = 99.4$ for $P < 0.01$.

Voxels with high negative loadings on the canonical image, i.e., relatively smaller FA values with reduced coherence, were located predominantly in anterior white matter, including frontal lobe white matter, anterior cingulated, and anterior corpus callosum. Additionally, temporal and parietal lobe and cerebellum white matter areas were involved (Table III, Fig. 1).

Effects for *temporo-parietal* and *frontal* β *coherence* were not significant (Wilk's lambda after transformation 2.17, 14 df, $P = 0.99$ and 5.73, 14 df, $P = 0.98$, respectively).

Healthy controls

Temporo-parietal α coherence. For the effect of temporo-parietal coherence we found eight eigenvectors having eigenvalues greater than unity. From MANOVA, Wilk's lambda after transformation corresponded to $\chi^2 = 18.18$ with 16 degrees of freedom, $P < 0.05$. The effect of coherence was almost completely accounted for by the second canonical image. Its canonical value was 53.87 and larger than the threshold $F_2^{14} = 19.4$ for $P < 0.05$.

Voxels with high negative loadings on the canonical image, i.e. relatively smaller FA values with reduced coherence, were located predominantly in posterior white matter, including temporal, parietal and occipital lobe white matter and posterior corpus callosum. Additionally, effects were found in brainstem and inferior frontal lobes (Table IV, Fig. 2).

Effects for *frontal* α and *temporo-parietal* and *frontal* β *coherence* were not significant (Wilk's lambda after transformation 16.49, 16 df, $P = 0.50$ for frontal α, 18.03, 16 df, $P = 0.50$ for temporo-parietal β and 21.16, 16 df, $P = 0.25$, for frontal β coherence).

MD Maps

MCI patients

Temporo-parietal α coherence. For the effect of temporo-parietal α coherence, we found five eigenvectors having eigenvalues greater than unity. From MANOVA, Wilk's lambda after transformation corresponded to $\chi^2 = 20.51$ with 10 degrees of freedom, $P < 0.025$. The effect of coherence was almost completely accounted for by the second canonical image. Its canonical value was 31.67 and larger than the threshold $F_2^{14} = 19.4$ for $P < 0.05$.

Voxels with high positive loadings on the canonical image, i.e., relatively increased MD values with reduced coherence, were located predominantly in posterior white matter, including, temporal, parietal and occipital lobe white matter, parahippocampal gyrus, and posterior corpus callosum. Additionally, effects were found in frontal lobe white matter, cerebellum, midbrain, and pons (Table V, Fig. 3).

Frontal α coherence. For the effect of frontal α coherence, we found five eigenvectors having eigenvalues greater than unity. From MANOVA, Wilk's lambda after transformation corresponded to $\chi^2 = 30.40$ with 10 degrees of freedom, $P < 0.001$. The effect of coherence was almost completely accounted for by the second canonical image.

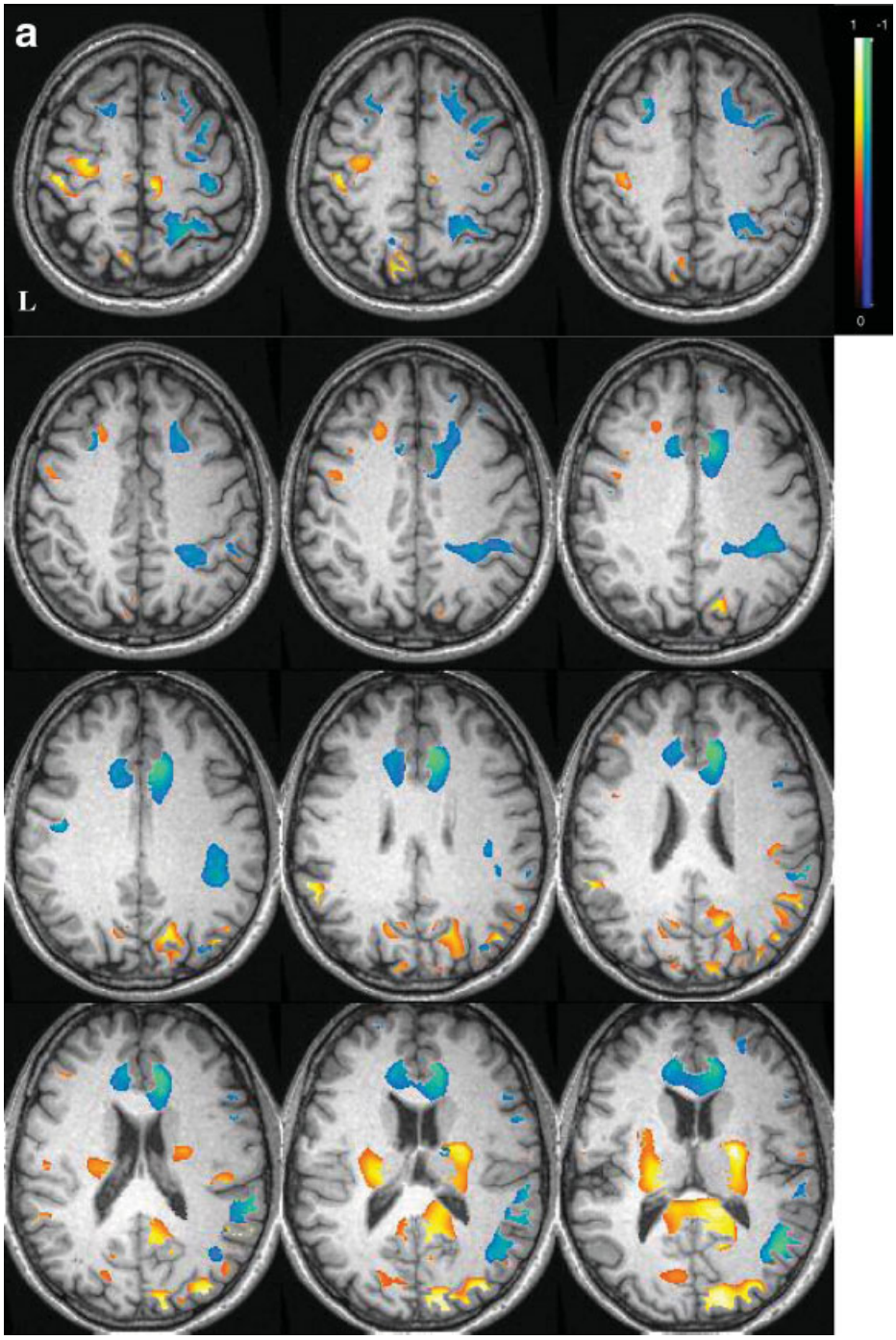

Figure 1.

Projection of the negative components of the canonical image into voxel space-posterior and frontal coherence in MCI patients, FA maps. (**a**) Axial sections: The canonical images derived from the FA maps for posterior and frontal coherence, respectively, in MCI patients in voxel space projected on the rendered axial sections of the T1-weighted template brain. Sections move from dorsal at Talairach–Tournoux coordinate $z = 57$ to ventral $z = -35$, sections are 4 mm apart. Right of image is right of brain (view from superior). L – left. (**b**) Midsagittal section: red to yellow: components of the canonical image for temporo-parietal coherence. Blue to green: components of the canonical images for frontal coherence.

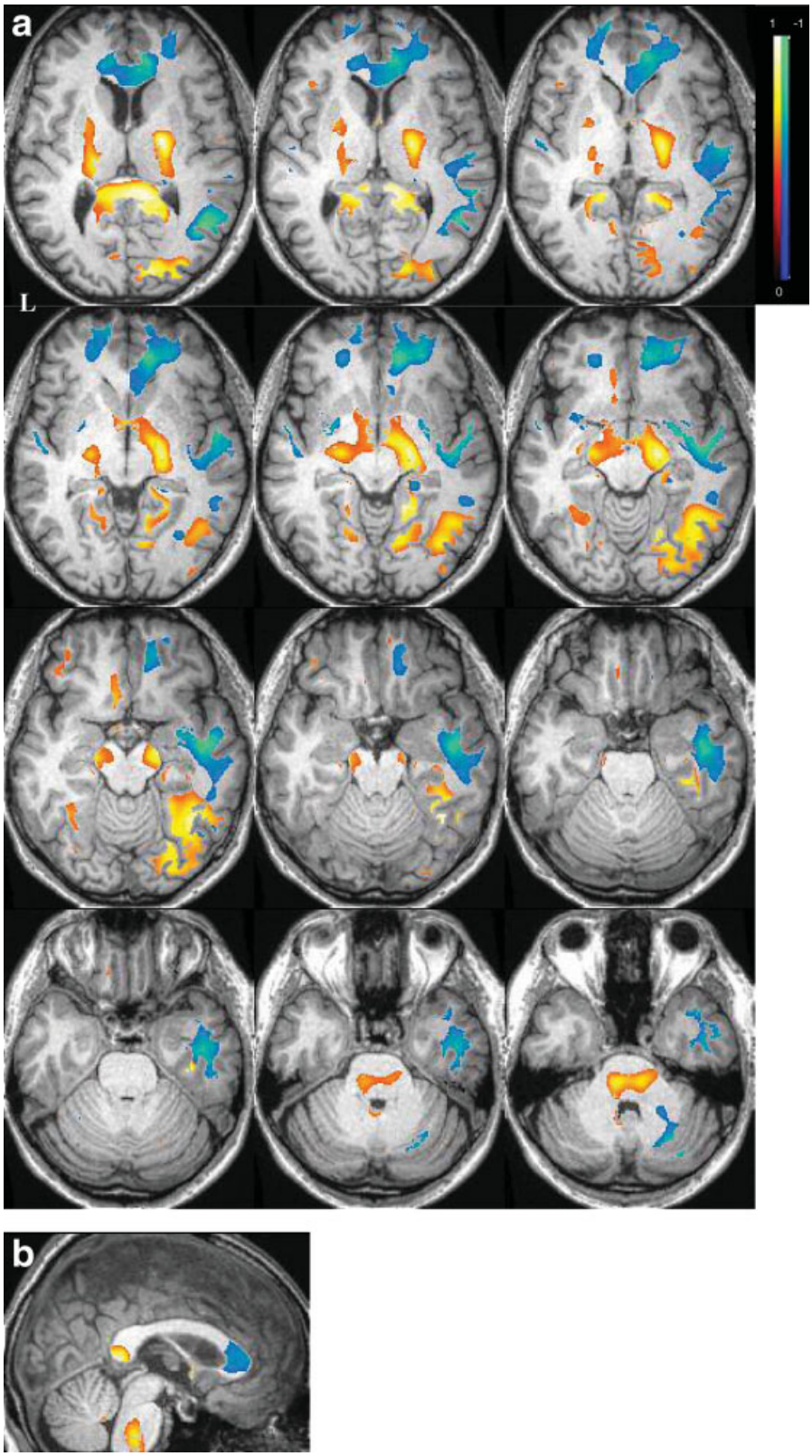

Figure 1. (Continued)

TABLE II. Voxel with negative peak loadings on the canonical image in MCI patients, posterior coherence, FA maps

Region	Side	Coordinates (mm)		
		x	*y*	*z*
Internal capsule	R	20	−9	10
Middle occipital gyrus WM	R	35	−85	20
Corpus callosum splenium	R	5	−41	7
Cuneus WM	R	13	−91	18
Fusiform gyrus WM	R	39	−56	−14
Pedunculus cerebri	R	19	−18	−6
Anterior cerebellum, culmen	R	15	−49	−5
Parahippocampal gyrus WM	R	36	−28	−21
Posterior cerebellum, inf. semilunar lobule	R	9	−58	−39
Lingual gyrus WM	R	21	−71	−8
Supramarginal gyrus WM	R	49	−53	22
Posterior cerebellum	R	13	−40	−37
Angular gyrus WM	R	46	−74	30
Precuneus WM	R	13	−72	34
Medial frontal gyrus WM	R	5	−26	53
Inferior occipital gyrus WM	R	39	−71	−5
Middle occipital gyrus WM	R	26	−84	−9
Posterior cerebellum, declive	R	38	−74	−22
Postcentral gyrus WM	L	−47	−21	52
Supramarginal gyrus WM	L	−63	−45	28
Thalamus, lateral posterior nucleus	L	−20	−21	12
Precentral gyrus WM	L	−30	−15	57
Pons	L	−7	−35	−33
Superior parietal lobule	L	−14	−71	53
Posterior cerebellum, tonsil	L	−10	−59	−35

Voxel with negative loading above the 95th percentile. Brain regions are indicated by Talairach and Tournoux coordinates, *x*, *y*, and *z* [Talairach and Tournoux, 1988]: *x*, the medial to lateral distance relative to midline (positive = right hemisphere); *y*, the anterior to posterior distance relative to the anterior commissure (positive = anterior); *z*, superior to inferior distance relative to the anterior commissure -posterior commissure line (positive = superior). WM, white matter; R/L, right/left.

Its canonical value was 81.2 and larger than the threshold $F_2^{14} = 19.4$ for $P < 0.05$.

Voxels with high positive loadings on the canonical image, i.e., relatively increased MD values with reduced coherence, were located predominantly in anterior white matter, including frontal lobe and anterior cingulate white matter, and anterior corpus callosum. Additionally, effects were found in posterior white matter, including temporal and parietal lobe white matter, posterior corpus callosum, cerebellum, and pons (Table VI and Fig. 3).

Effects for *temporo-parietal* and *frontal* β *coherence* were not significant (Wilk's lambda after transformation 2.08, 10 df, $P = 0.99$ and 2.73, 10 df, $P = 0.99$, respectively).

Healthy controls

Temporo-parietal* α *coherence. For the effect of temporo-parietal α coherence, we found six eigenvectors having eigenvalues greater than unity. From MANOVA, Wilk's lambda after transformation corresponded to $\chi^2 = 35.17$ with 12 degrees of freedom, $P < 0.001$. The effect of coherence was almost completely accounted for by the second canonical image. Its canonical value was 78.01 and larger than the threshold $F_2^{18} = 19.4$ for $P < 0.05$.

Voxels with high positive loadings on the canonical image, i.e., relatively increased MD values with reduced coherence, were located predominantly in posterior white matter, including temporal, parietal and occipital lobe white matter and parahippocampal gyrus. Additionally, effects were found in frontal lobe white matter, midbrain and cerebellum. Corpus callosum was not involved in the effects (Table VII and Fig. 4).

Effects for *frontal* α and *temporo-parietal* and *frontal* β *coherence* were not significant (Wilk's lambda after transformation 9.26, 12 df, $P = 0.75$ for frontal α, 10.42, 12 df, $P = 0.75$ for temporo-parietal β and 14.75, 12 df, $P = 0.50$, for frontal β coherence).

DISCUSSION

In this study we investigated the association between interhemispheric coherence in EEG and fiber tract integrity in the cerebral white matter determined using DTI in sub-

TABLE III. Voxel with negative peak loadings on the canonical image in MCI patients, frontal coherence, FA maps

Region	Side	Coordinates (mm)		
		x	*y*	*z*
Anterior cingulate gyrus WM	R	6	28	24
Middle temporal gyrus WM	R	46	−62	12
Posterior cerebellum, tonsil	R	30	−55	−40
Middle temporal gyrus WM	R	45	−11	−11
Medial frontal gyrus WM	R	11	41	−7
Superior temporal gyrus WM	R	63	−43	18
Superior parietal lobule WM	R	24	−53	62
Superior temporal gyrus WM	R	55	−1	−5
Superior temporal gyrus WM	R	58	−41	7
Extranuclear WM	R	28	−4	−10
Middle frontal gyrus WM	R	25	44	−10
Middle frontal gyrus WM	R	38	10	51
Superior temporal gyrus WM	R	39	13	−32
Supramarginal gyrus WM	R	42	−41	33
Precentral gyrus WM	R	34	−21	56
Medial frontal gyrus WM	L	−10	64	−6
Middle frontal gyrus WM	L	−30	19	41
Middle temporal gyrus	L	−60	0	−6
Precentral gyrus WM	L	−48	−11	30
Anterior cingulate gyrus WM	L	−11	41	7

Voxel with negative loading above the 95th percentile. Brain regions are indicated by Talairach and Tournoux coordinates, *x*, *y*, and *z* [Talairach and Tournoux, 1988]: *x*, the medial to lateral distance relative to midline (positive = right hemisphere); *y*, the anterior to posterior distance relative to the anterior commissure (positive = anterior); *z*, superior to inferior distance relative to the anterior commissure -posterior commissure line (positive = superior). WM, white matter; R/L, right/left.

TABLE IV. Voxel with negative peak loadings on the canonical image in controls, temporo-parietal coherence, FA maps

Region	Side	Coordinates (mm)		
		x	*y*	*z*
Inferior parietal lobule WM	R	50	−25	28
Precentral gyrus WM	R	32	−18	51
Precentral gyrus WM	R	44	−6	41
Inferior frontal gyrus WM	R	43	22	4
Posterior cingulate gyrus WM	R	17	−49	28
Corpus callosum splenium	R	2	−35	21
Cuneus WM	R	9	−90	9
Medial temporal gyrus WM	R	25	−59	23
Postcentral gyrus WM	R	55	−10	23
Cuneus WM	R	19	−87	19
Medial occipital gyrus WM	R	42	−65	−8
Internal capsule	R	16	−11	3
Superior frontal gyrus WM	R	15	19	48
Lingual gyrus WM	R	19	−73	−5
Inferior frontal gyrus WM	R	45	12	11
Inferior temporal gyrus WM	R	55	−55	−3
Cingulate gyrus WM	L	−18	−30	26
Precentral gyrus WM	L	−45	−8	53
Brainstem, medulla WM	L	−5	−37	−41
Precentral gyrus WM	L	−54	−3	22

Voxel with negative loading above the 95th percentile. Brain regions are indicated by Talairach and Tournoux coordinates, *x*, *y*, and *z* [Talairach and Tournoux, 1988]: *x*, the medial to lateral distance relative to midline (positive = right hemisphere); *y*, the anterior to posterior distance relative to the anterior commissure (positive = anterior); *z*, superior to inferior distance relative to the anterior commissure -posterior commissure line (positive = superior). WM, white matter; R/L, right/left.

jects with amnestic MCI and cognitively and physically healthy controls. We found a pattern of predominant posterior white matter tracts associated with temporo-parietal α coherence in MCI patients and controls. Additionally, in MCI patients frontal α coherence was associated with integrity of predominantly frontal fiber tracts. Effects for β coherence in MCI subjects and controls and effects for frontal α coherence in controls were not significant.

In contrast to results of three earlier studies [Jelic et al., 1996, 2000; Jiang and Zheng, 2006], we found significantly reduced coherences in the α-band in the MCI patients in posterior association cortex. The association cortex is a very vulnerable region in the development of AD [Delbeuck et al., 2003; Hampel et al., 2002] and therefore a decline of coherence would match an early stage of AD. Overall, our MCI and control groups were considerably older than the sample of the two previous studies. An average age of 62 in the MCI patients of one previous study [Jelic et al., 1996] suggests a low risk of AD in this sample as conversion into AD in MCI has been found associated with higher age in several studies [Maioli et al., 2007]. In the other study [Jelic et al., 2000], the MCI patients were relatively young (58 years), as well. However, half of the patients had converted to AD. The coherence values in these patients lay between those of the AD and the control groups, but neither difference (MCI vs. AD, MCI vs. controls) reached statistical significance [Jelic et al., 2000].

Temporo-parietal interhemispheric coherence was correlated with a predominantly posterior network of FA and MD values, including posterior corpus callosum, occipital, parietal and temporal lobes white matter, and white matter areas of the thalamus, midbrain, pons, and cerebellum, both in MCI subjects and controls. Additionally, frontal lobe areas, including precentral gyrus and dorsolateral prefrontal cortex white matter, were involved.

Interhemispheric coherence depends on the integrity of intracortical and subcortical fiber systems [Saltzberg et al., 1986]. During childhood and adolescence coherence increases nonlinearly [Marosi et al., 1992; Schmid et al., 1992; Stam et al., 2000; Thatcher, 1992]. These changes may reflect the maturation of brain organization through myelo- and synapto-genesis. DTI-based measures of FA and MD have been shown to be sensitive towards changes in fiber tract integrity [Beaulieu, 2002]. Therefore, we hypothesize that the correlation between interhemispheric coherence and diffusion measures reveals fiber systems contributing to the maintenance of interhemispheric coherence in the human brain.

Our data on the correlation between posterior coherence and posterior corpus callosum fiber tract integrity agree with independent evidence that the integrity of interhemispheric fiber systems crossing through the corpus callosum influences interhemispheric coherence [Pogarell et al., 2005]. Thus, reductions of interhemispheric coherence reflect the degree of anatomical section produced by surgical partial callosotomy [Montplaisir et al., 1990].

But the effects extended far beyond the corpus callosum in our study. Thatcher et al. [1986] have proposed a two compartmental model to describe the spatial distribution of intrahemispheric and interhemispheric coherences incorporating phase delays as a function of interelectrode distance. The two compartments were supposed to reflect short- and long-distance cortico–cortical connections, respectively. However, this model would also agree with a contribution of subcortical centers modulating interhemispheric coherence. Consistently, more recent approaches in modelling essential features of the EEG signal incorporate thalamocortical projections [Robinson, 2003; Robinson et al., 2003]. For the visual system experiments in monkeys have suggested feedback loops between the primary visual cortex and the dorsolateral geniculate nucleus of the thalamus that tune the thalamic excitatory activity on cortical target areas [Sillito et al., 1994]. In patients with Parkinson's disease intrasurgical recordings showed a high coherence between local field potentials in the thalamus and cortical EEG supporting an important role of the thalamus in synchronization of the electrical activity between distant cortical areas [Sarnthein and Jeanmonod, 2007]. In patients with acquired immunodeficiency syndrome coherence in the upper θ and lower α band was correlated with metabolic activity in the thalamus and basal ganglia determined using FDG-PET [Newton et al., 1993].

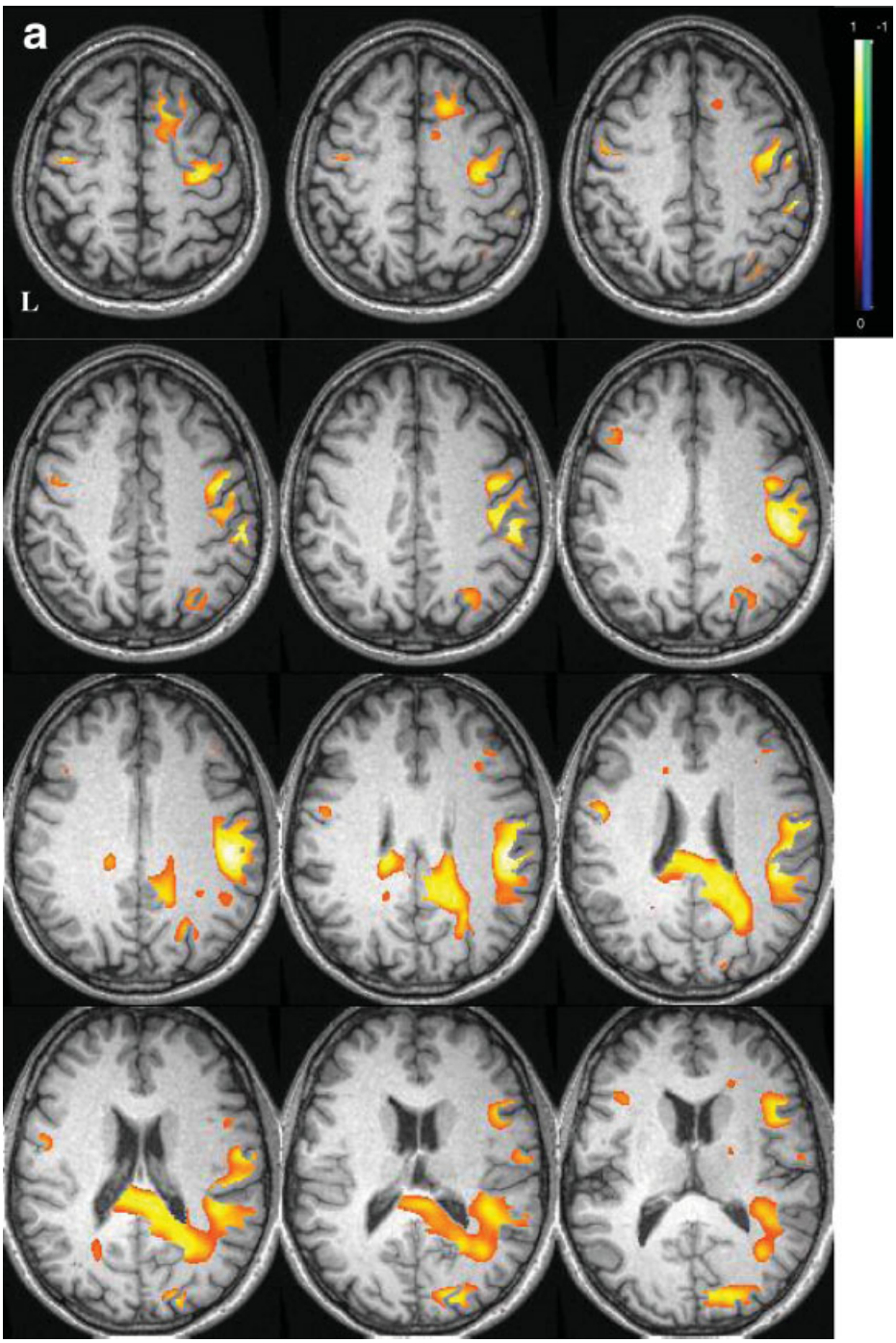

Figure 2.

Projection of the negative components of the canonical image into voxel space -temporo-parietal coherence in healthy controls, FA maps. (**a**) Axial sections: The canonical images derived from the FA maps for temporo-parietal coherence in healthy control subjects in voxel space projected on the rendered axial sections of the T1-weighted template brain. Sections move from dorsal at Talairach–Tournoux coordinate $z = 57$ to ventral $z = -35$, sections are 4 mm apart. Right of image is right of brain (view from superior). L, left. (**b**) Midsagittal section.

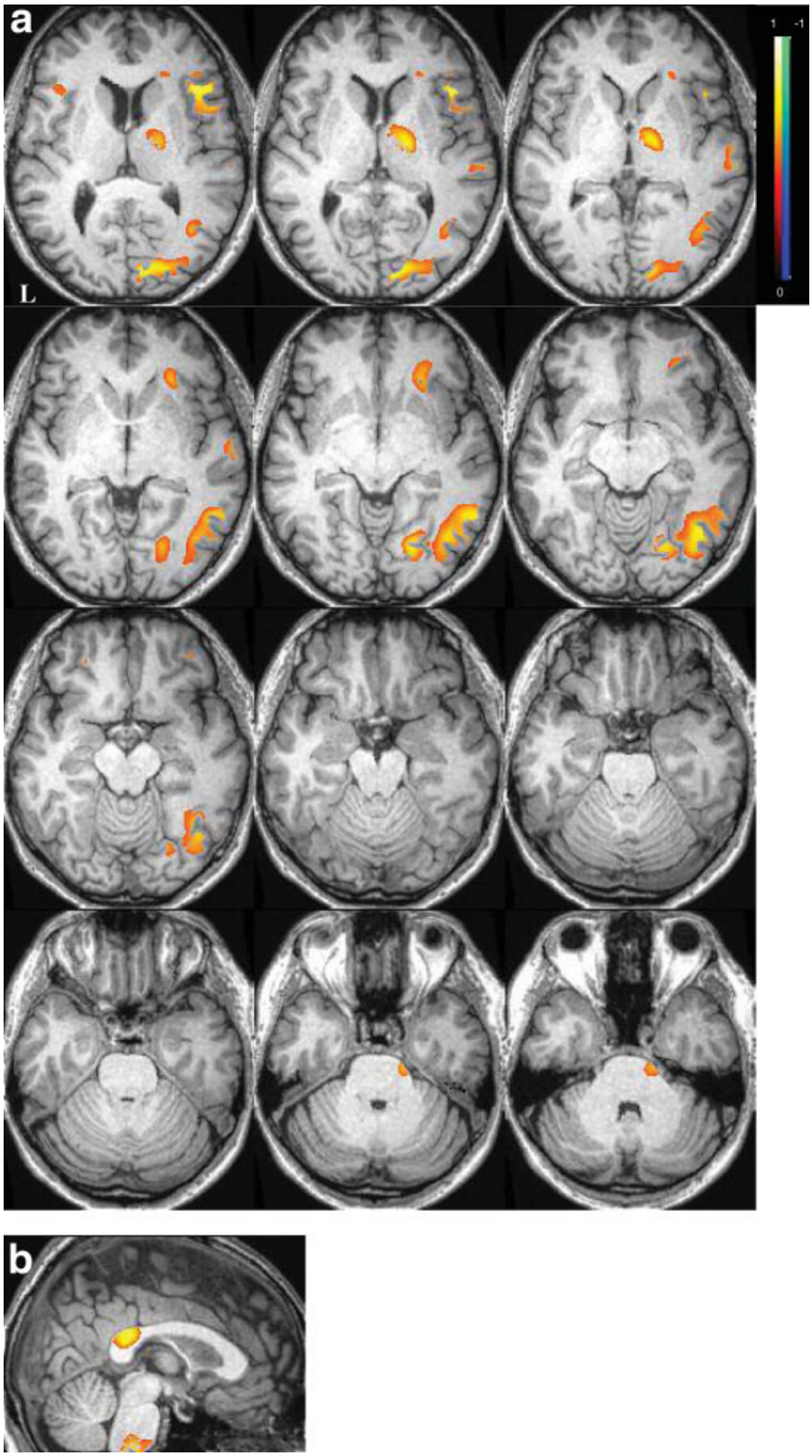

Figure 2. (Continued)

TABLE V. Voxel with positive peak loadings on the canonical image in MCI patients, temporo-parietal coherence, MD maps

Region	Side	Coordinates (mm)		
		x	*y*	*z*
Midbrain	R	19	−22	−1
Anterior cerebellum, culmen	R	19	−45	−22
Posterior cerebellum, inf. semi-lunar lobule	R	27	−64	−39
Posterior cingulate gyrus WM	R	9	−49	12
Posterior cerebellum, tonsil	R	17	−49	−33
Posterior cerebellum, uvula	R	10	−68	−34
Pons	R	2	−30	−28
Precuneus WM	R	15	−66	25
Corpus callosum splenium	R	29	−32	17
Posterior cerebellum, pyramis	L	−14	−69	−29
Anterior cerebellum, culmen	L	−32	−54	−23
Posterior cerebellum, tonsil	L	−35	−57	−33
Superior frontal gyrus WM	L	−39	51	−17
Precentralgyrus WM	L	−39	4	37
Superior frontal gyrus WM	L	−29	42	−16
Midbrain	L	−13	−30	−9
Middle frontal gyrus WM	L	−40	56	−8
Precuneus WM	L	−23	−69	24
Lingual gyrus WM	L	−23	−50	−2
Pons	L	−16	−28	−28
Parahippocampal gyrus WM	L	−20	−50	6
Inferior temporal gyrus WM	L	−51	−33	−17

Voxel with negative loading above the 95th percentile. Brain regions are indicated by Talairach and Tournoux coordinates, *x*, *y*, and *z* [Talairach and Tournoux, 1988]: *x*, the medial to lateral distance relative to midline (positive = right hemisphere); *y*, the anterior to posterior distance relative to the anterior commissure (positive = anterior); *z*, superior to inferior distance relative to the anterior commissure -posterior commissure line (positive = superior). WM, white matter; R/L, right/left.

The component extracted from FA maps that was significantly associated with posterior coherence in the α band additionally encompassed white matter areas in the midbrain and pons. This agrees with a large range of animal studies suggesting that cortical activation is elicited by brainstem reticular core stimulation, including the mesencephalic and pontine reticular formation [Frasch et al., 2007; Morgane et al., 1981; Steriade, 1995]. In patients with Parkinson's disease intracortical coherence was modulated by levodopa, suggesting a role of mesencephalic dopaminergic projections [Cassidy and Brown, 2001]. Evidence on cerebellar effects on intracortical coherence is more limited. In precise motor tasks, significant coherence has been shown between single units activity in deep cerebellar nuclei and local field potentials in primary motor cortex in monkeys [Soteropoulos and Baker, 2006]. In a MEG study on patients with Wilson's disease the tremor frequency related activity in primary motor cortex was significantly coupled with the activity of the ipsilateral thalamus and the contralateral cerebellum [Sudmeyer et al., 2006]. Therefore, our findings agree with previous evidence on a cerebellar effect on cortical EEG pattern that is mediated by thalamic nuclei.

The specificity of our results is underscored by the dissociation between effects for frontal and temporo-parietal coherence. Frontal coherence was associated with a predominantly frontal pattern of diffusivity comprising anterior corpus callosum, prefrontal cortex, and anterior cingulate gyrus. Additionally, temporal and parietal lobe areas as well as posterior corpus callosum were involved. The predominant contribution of anterior corpus callosum to frontal and posterior corpus callosum to temporo-parietal coherence agrees with an anterior-posterior topology of fiber systems passing through the corpus callosum as suggested by a wide range of animal and human studies [De Lacoste et al., 1985; Pandya and Seltzer, 1986; Schaltenbrand et al., 1970]. The contribution of fiber tract integrity in subcortical centers such as thalamus and cerebellum was less pronounced for frontal coherence than for temporo-parietal coherence. This may be related to the fact that the α rhythm is dominant in posterior cortex [Nunez et al., 2001]. More specifically, in a causal model wide reaching spread of α power was directed from posterior to frontal [Wang et al., 1992].

The observation that effects were more pronounced in MCI subjects than in controls and that effects of frontal coherence were only present in MCI but not in controls meets our original assumption that predementia AD pathology in at least some of our MCI subjects would induce variation in the same direction in both, coherence and fiber tract integrity. This would facilitate the detection of significant correlations between both measures. This is analogous to a classical neuropsychological lesion study: a lesion to a certain brain region will lead to specific cognitive impairment. The effect will be stronger if the lesion is more severe leading to a high correlation between the degree of impairment of the brain structure and cognitive performance.

We found significant correlations between diffusion measures and interhemispheric coherence in the α, but not the β band. We do not have a final explanation for this observation. It may be important that both frontal and temporo-parietal coherences were significantly smaller in the β than the α band for both MCI subjects and controls (univariate ANOVA with repeated measures factor frequency band and diagnosis as between subjects factor: differences in α and β band were significant for frontal coherence with $F^1_{34} = 55.4$, $P < 0.001$, without significant interaction of frequency band by diagnosis with $F^1_{34} = 2.7$, $P = 0.11$, and for temporo-parietal coherence with $F^1_{34} = 12.9$, $P < 0.001$, with significant interaction of frequency band by diagnosis with $F^1_{34} = 6.9$, $P < 0.02$). Variability of coherence measures was higher for the β than the α band: the coefficient of variation was 0.43 and 0.45 for the frontal and temporo-parietal coherence, respectively, in the α band, and 0.75 and 1.09 for the frontal and temporo-parietal coherence, respectively, in the β band. This higher variation may have masked potential correlations between β band

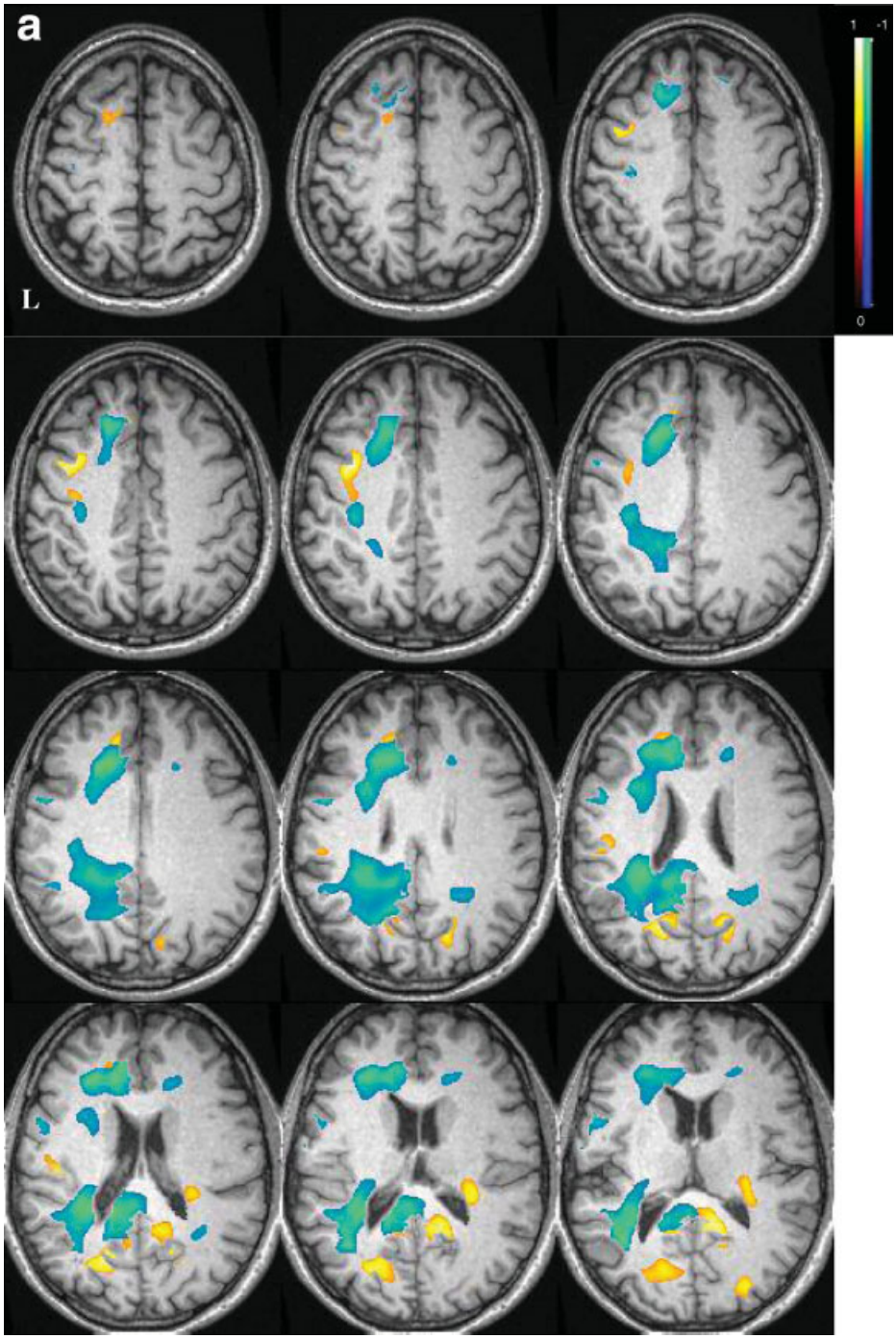

Figure 3.

Projection of the positive components of the canonical image into voxel space -temporo-parietal and frontal coherence in MCI patients, MD maps. (**a**) Axial sections: The canonical images derived from the MD maps for posterior and frontal coherence, respectively, in MCI patients in voxel space projected on the rendered axial sections of the T1-weighted template brain. Sections move from dorsal at Talairach–Tournoux coordinate $z = 57$ to ventral $z = -35$, sections are 4 mm apart. Right of image is right of brain (view from superior). L, left. (**b**) Midsagittal section: red to yellow: components of the canonical image for temporo-parietal coherence. Blue to green: components of the canonical images for frontal coherence.

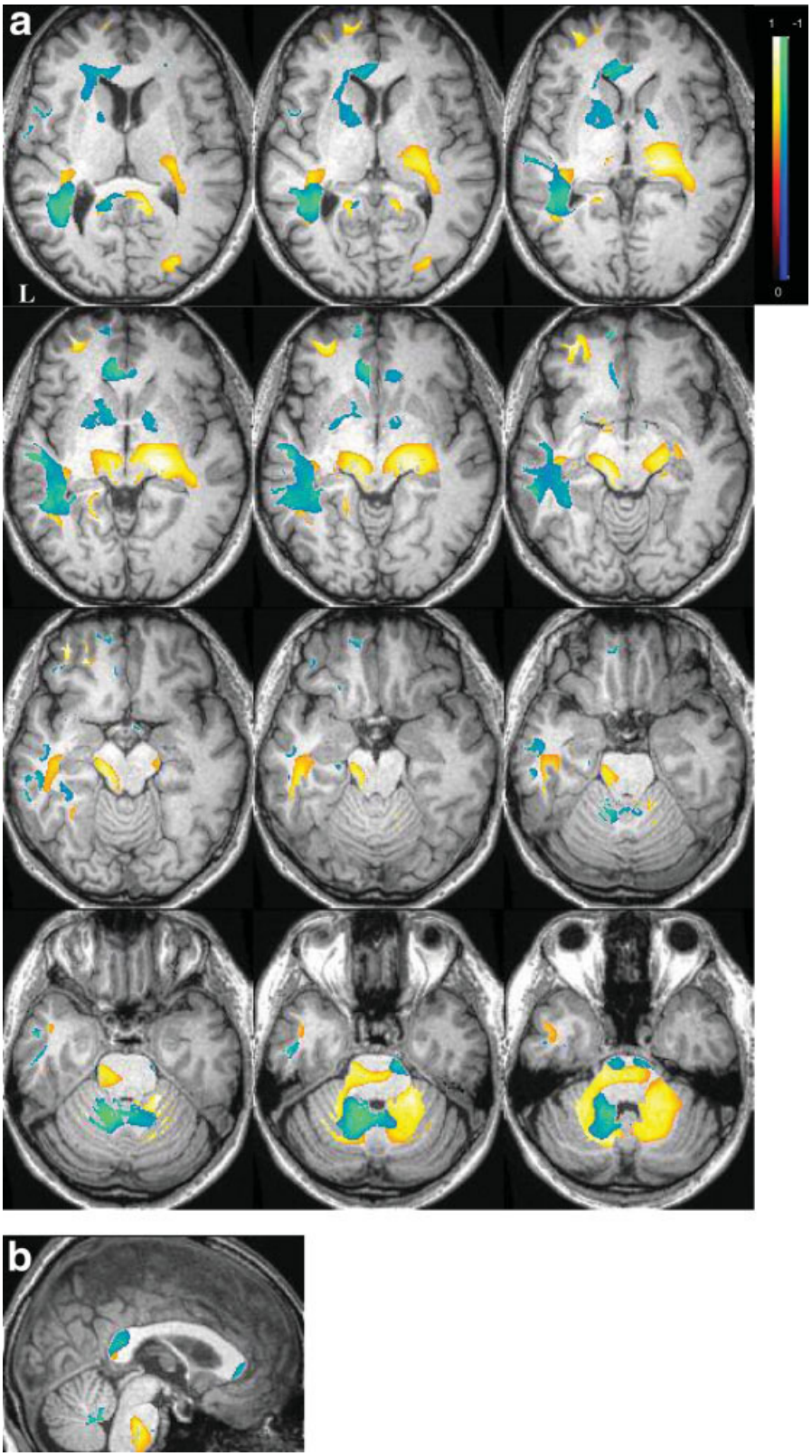

Figure 3. (Continued)

TABLE VI. Voxel with positive peak loadings on the canonical image in MCI patients, frontal coherence, MD maps

Region	Side	Coordinates (mm)		
		x	*y*	*z*
Pons	R	11	−22	−27
Anterior cerebellum, dentate	L	−14	−56	−22
Corpus callosum splenium	L	−17	−43	21
Middle frontal gyrus WM	L	−22	22	29
Anterior cingulate gyrus WM	L	−11	39	17
Anterior cingulate gyrus WM	L	−17	32	17
Middle frontal gyrus WM	L	−29	31	17
Middle temporal gyrus WM	L	−42	−59	15
Capsula extrema	L	−34	−40	20
Middle temporal gyrus WM	L	−38	−48	9
Middle temporal gyrus WM	L	−58	−18	−3
Superior frontal gyrus WM	L	−11	58	−12
Anterior cingulate gyrus WM	L	−7	34	−8
Frontal lobe WM	L	−20	25	39
Middle temporal gyrus WM	L	−51	−47	1
Fusiform gyrus WM	L	−60	−15	−26
Superior frontal gyrus WM	L	−15	53	−23
Middle temporal gyrus WM	L	−60	−40	−9
Inferior frontal gyrus WM	L	−35	9	23
Posterior cingulate gyrus WM	L	−19	−56	26
Precentral gyrus WM	L	−54	2	26
Frontal lobe WM	L	−38	−25	35
Precentral gyrus WM	L	−59	12	8

Voxel with negative loading above the 95th percentile. Brain regions are indicated by Talairach and Tournoux coordinates, *x*, *y*, and *z* [Talairach and Tournoux, 1988]: *x*, the medial to lateral distance relative to midline (positive = right hemisphere); *y*, the anterior to posterior distance relative to the anterior commissure (positive = anterior); *z*, superior to inferior distance relative to the anterior commissure -posterior commissure line (positive = superior).
WM, white matter; R/L, right/left.

coherence and diffusion measures. We have investigated EEG recordings of wakeful resting subjects with eyes closed. The waking state is characterized by the predominance of a temporo-occipital background activity within the α frequency band, whereas faster frequencies, such as β and γ, that are indicators of an activation state, are less pronounced [Laufs et al. 2003a, 2003b; Miller, 2007]. EEG signals at higher frequencies are smaller in amplitudes, exhibit a reduced signal-to-noise ratio and are susceptible to contamination by artifacts. These factors may have contributed to both lower values and higher variabilities of β coherences [Miller, 2007; Nunez et al., 1997, 1999].

Several reports suggest that alpha rhythms are composed of at least two different sub-rhythms at lower (about 8–10 Hz) and higher frequency (about 10–12 Hz), which are related to trait markers of cognitive performance [Klimesch, 1997] and respond to task performance [Klimesch, et al., 2005]. As we studied subjects in a wakeful resting state we did not differentiate between alpha sub-rhythms. However, it will be very interesting in future to study the association of fiber tract integrity with inter- and intrahemispheric coherence during task performance. This might also help to better understand the morphological basis of alpha sub-rhythms and their association with cognitive task performance.

In interpreting the results of our study, one has to consider one important issue. The multivariate approach revealed a network of brain areas that were correlated among each other and at the same time were correlated with interhemispheric coherence. We can not, however, state, which parts of this network are causally involved in the maintenance of interhemispheric coherence. To date, our knowledge on the underlying substrate of interhemispheric coherence arises mainly from findings in lesion studies in animals, correlations between functional connectivity from PET studies in patients, source localization from EEG or MEG data, and intrasurgical recordings of thalamic activity in patients. Our study provides a methodology to access the fiber tracts underlying interhemispheric connectivity in the living human brain. One could

TABLE VII. Voxel with positive peak loadings on the canonical image in controls, temporo-parietal coherence, MD maps

Region	Side	Coordinates (mm)		
		x	*y*	*z*
Midbrain	R	2	−33	−18
Midbrain	R	17	−20	−8
Anterior cingulate gyrus WM	R	5	45	4
Inferior temporal lobe WM	R	35	0	−24
Inferior temporal lobe WM	R	55	−3	−31
Fusiform gyrus WM	L	−35	−39	−15
Temporal lobe WM (uncinate fasciculus)	L	−32	−5	−12
Parahippocampal gyrus WM	L	−27	−12	−26
Middle occipital gyrus WM	L	−24	−86	14
Sublobar WM (occipitofrontal fasciculus)	L	−34	−44	18
Cuneus WM	L	−11	−79	23
Temporal lobe WM	L	−41	−48	2
Middle temporal gyrus WM	L	−58	−1	−24
Postcentral gyrus WM	L	−42	−27	43
Insula WM	L	−43	−18	−6
Precentral gyrus WM	L	−36	−11	46
Medial frontal gyrus WM	L	−9	49	0
Postcentral gyrus WM	L	−55	−30	49
Anterior cerebellum, culmen	L	−9	−38	−7
Lingual gyrus WM	L	−18	−62	0
Middle occipital gyrus WM	L	−31	−71	5
Medial frontal gyrus WM	L	−7	−17	63
Postcentral gyrus WM	L	−56	−17	29
Middle occipital gyrus WM	L	−43	−83	10

Voxel with negative loading above the 95th percentile. Brain regions are indicated by Talairach and Tournoux coordinates, *x*, *y*, and *z* [Talairach and Tournoux, 1988]: *x*, the medial to lateral distance relative to midline (positive = right hemisphere); *y*, the anterior to posterior distance relative to the anterior commissure (positive = anterior); *z*, superior to inferior distance relative to the anterior commissure -posterior commissure line (positive = superior).
WM, white matter; R/L, right/left.

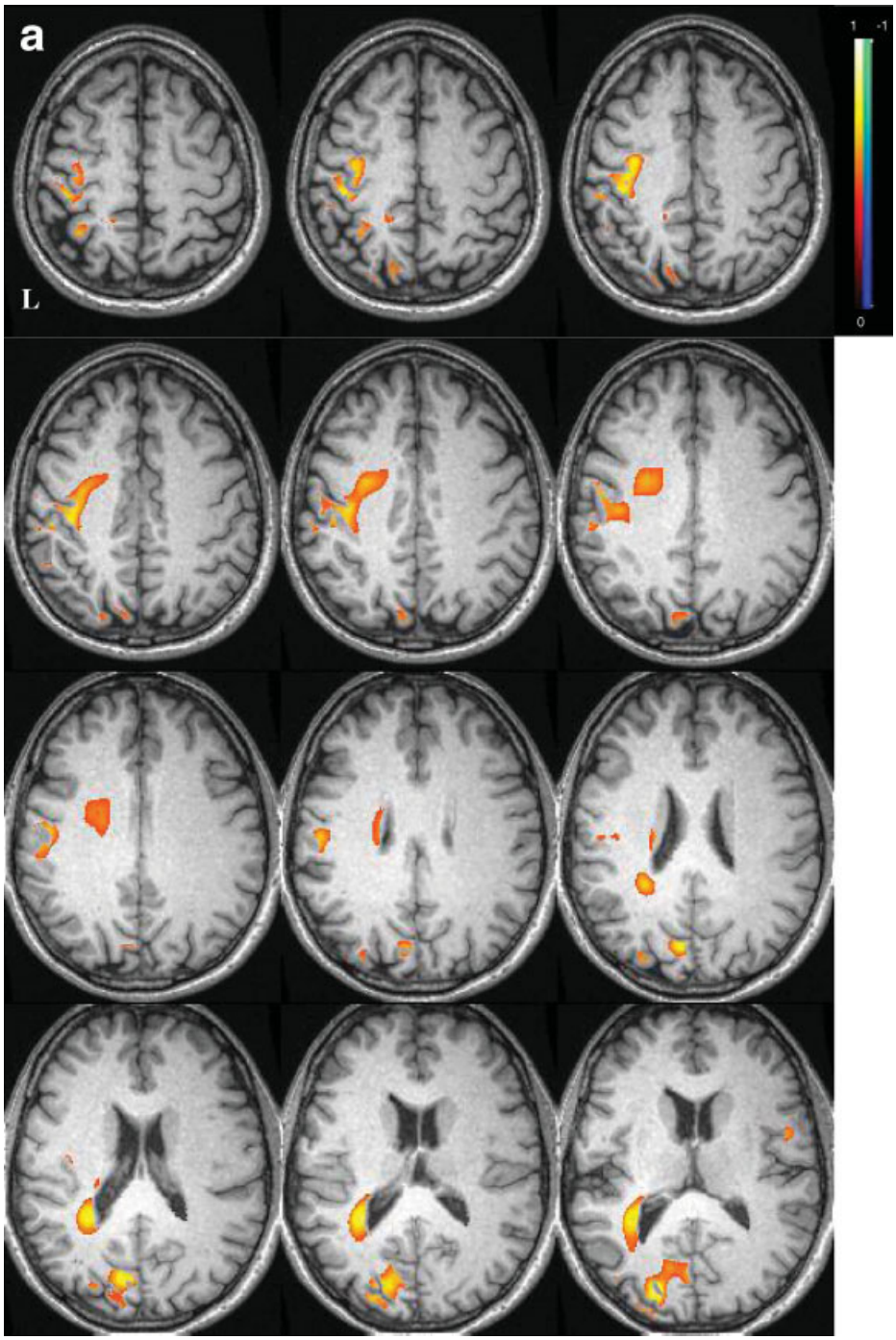

Figure 4.

Projection of the positive components of the canonical image into voxel space -temporo-parietal coherence in controls, MD maps. (**a**) Axial sections: The canonical images derived from the MD maps for temporo-parietal coherence in healthy control subjects in voxel space projected on the rendered axial sections of the T1-weighted template brain. Sections move from dorsal at Talairach-Tournoux coordinate $z = 57$ to ventral $z = -35$, sections are 4 mm apart. Right of image is right of brain (view from superior). L, left. (**b**) Midsagittal section.

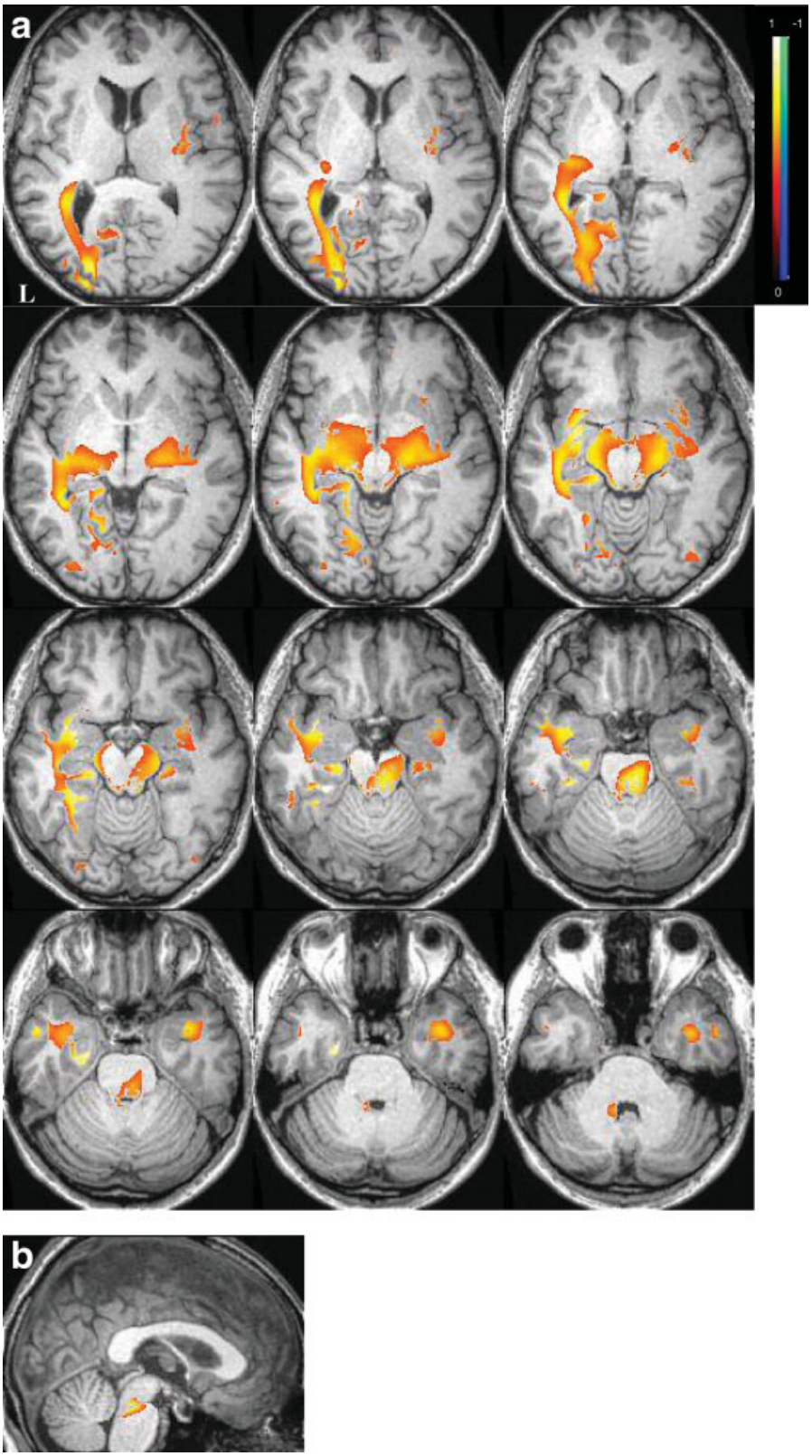

Figure 4. (Continued)

use the regional pattern that has been identified in our sample to extract the FA values from these locations in an independent sample and feed them into a path model to assess direct and indirect effects of certain regions on interhemispheric coherence.

According to previous studies, the functional coupling of resting EEG in subjects with MCI or AD might be more affected between frontal and parietal regions than between the hemispheres [Babiloni et al., 2006; Koenig et al., 2005; Prichep, 2007; Rossini et al., 2006, 2008]. Therefore, it would be worthwhile to investigate the association between intrahemispheric coherence and fiber tract integrity in future studies.

In summary, we found specific associations between interhemispheric coherence and the integrity of cortical and subcortical white matter tracts. The results of our study suggest that networks involving corpus callosum, thalamus, mesencephalic and pontine white matter and cerebellum may underlay the maintenance of interhemispheric coherence. The paradigm presented here to combine electrophysiological measures of cortical coupling and DTI-based measurement of fiber tract integrity may prove useful in future research on the structural basis of brain function. Presently, we are collecting data on patients with AD, as we expect even stronger effects in the presence of manifest impairment of intracortical connectivity and fiber tract integrity as induced by clinically manifest AD. Through clinical follow-up of our MCI subjects we will be able to assess the diagnostic accuracy of coherence and diffusivity measures to predict the conversion into AD.

REFERENCES

Ashburner J, Friston K (1997): Multimodal image coregistration and partitioning–a unified framework. Neuroimage 6:209–217.

Ashburner J, Friston KJ (2000): Voxel-based morphometry–The methods. Neuroimage 11(6 Part 1):805–821.

Ashburner J, Neelin P, Collins DL, Evans A, Friston K (1997): Incorporating prior knowledge into image registration. Neuroimage 6:344–352.

Ashburner J, Andersson JL, Friston KJ (1999): High-dimensional image registration using symmetric priors. Neuroimage 9(6 Part 1):619–628.

Babiloni F, Babiloni C, Fattorini L, Carducci F, Onorati P, Urbano A (1995): Performances of surface Laplacian estimators: A study of simulated and real scalp potential distributions. Brain Topogr 8:35–45.

Babiloni C, Ferri R, Binetti G, Cassarino A, Dal Forno G, Ercolani M, Ferreri F, Frisoni GB, Lanuzza B, Miniussi C, Nobili F, Rodriguez G, Rundo F, Stam CJ, Musha T, Vecchio F, Rossini PM (2006): Fronto-parietal coupling of brain rhythms in mild cognitive impairment: A multicentric EEG study. Brain Res Bull 69:63–73.

Backman L, Almkvist O, Nyberg L, Andersson J (2000): Functional changes in brain activity during priming in Alzheimer's disease. J Cogn Neurosci 12:134–141.

Barry RJ, Clarke AR, McCarthy R, Selikowitz M, Johnstone SJ, Rushby JA (2004): Age and gender effects in EEG coherence. I. Developmental trends in normal children. Clin Neurophysiol 115:2252–2258.

Barry RJ, Clarke AR, McCarthy R, Selikowitz M, Johnstone SJ, Hsu CI, Bond D, Wallace MJ, Magee CA (2005): Age and gender effects in EEG coherence. II. Boys with attention deficit/hyperactivity disorder. Clin Neurophysiol 116:977–984.

Barry RJ, Clarke AR, McCarthy R, Selikowitz M (2006): Age and gender effects in EEG coherence. III. Girls with attention-deficit/hyperactivity disorder. Clin Neurophysiol 117:243–251.

Beaulieu C (2002): The basis of anisotropic water diffusion in the nervous system—A technical review. NMR Biomed 15:435–455.

Berres M, Monsch AU, Bernasconi F, Thalmann B, Stahelin HB (2000): Normal ranges of neuropsychological tests for the diagnosis of Alzheimer's disease. Stud Health Technol Inform 77:195–199.

Bokde AL, Lopez-Bayo P, Meindl T, Pechler S, Born C, Faltraco F, Teipel SJ, Moller HJ, Hampel H (2006): Functional connectivity of the fusiform gyrus during a face-matching task in subjects with mild cognitive impairment. Brain 129(Part 5):1113–1124.

Bookheimer SY, Strojwas MH, Cohen MS, Saunders AM, Pericak-Vance MA, Mazziotta JC, Small GW (2000): Patterns of brain activation in people at risk for Alzheimer's disease. N Engl J Med 343:450–456.

Bozzali M, Falini A, Franceschi M, Cercignani M, Zuffi M, Scotti G, Comi G, Filippi M (2002): White matter damage in Alzheimer's disease assessed in vivo using diffusion tensor magnetic resonance imaging. J Neurol Neurosurg Psychiatry 72: 742–746.

Brun A, Englund E (1986): A white matter disorder in dementia of the Alzheimer type: A pathoanatomical study. Annals Neurol 19:253–262.

Busse A, Hensel A, Guhne U, Angermeyer MC, Riedel-Heller SG (2006): Mild cognitive impairment: Long-term course of four clinical subtypes. Neurology 67:2176–2185.

Cassidy M, Brown P (2001): Task-related EEG-EEG coherence depends on dopaminergic activity in Parkinson's disease. Neuroreport 12:703–707.

Chen P, Ratcliff G, Belle SH, Cauley JA, DeKosky ST, Ganguli M (2000): Cognitive tests that best discriminate between presymptomatic AD and those who remain nondemented. Neurology 55:1847–1853.

De Lacoste MC, Kirkpatrick JB, Ross ED (1985): Topography of the human corpus callosum. J Neuropath Exper Neurol 44:578–591.

Delbeuck X, Van der Linden M, Collette F (2003): Alzheimer's disease as a disconnection syndrome? Neuropsychol Rev 13: 79–92.

Devanand DP, Folz M, Gorlyn M, Moeller JR, Stern Y (1997): Questionable dementia: Clinical course and predictors of outcome. J Am Geriatr Soc 45:321–328.

Fellgiebel A, Wille P, Muller MJ, Winterer G, Scheurich A, Vucurevic G, Schmidt LG, Stoeter P (2004): Ultrastructural hippocampal and white matter alterations in mild cognitive impairment: A diffusion tensor imaging study. Dement Geriatr Cogn Disord 18:101–108.

Fellgiebel A, Muller MJ, Wille P, Dellani PR, Scheurich A, Schmidt LG, Stoeter P (2005): Color-coded diffusion-tensor-imaging of posterior cingulate fiber tracts in mild cognitive impairment. Neurobiol Aging 26:1193–1198.

Fellgiebel A, Dellani PR, Greverus D, Scheurich A, Stoeter P, Muller MJ (2006): Predicting conversion to dementia in mild cognitive impairment by volumetric and diffusivity measurements of the hippocampus. Psychiatry Res 146:283–287.

Fillenbaum GG, Peterson B, Morris JC (1996): Estimating the validity of the clinical Dementia Rating Scale: The CERAD experience. Consortium to Establish a Registry for Alzheimer's Disease. Aging (Milano) 8:379–385.

Folstein MF, Folstein SE, McHugh PR (1975): Mini-mental-state: A practical method for grading the cognitive state of patients for the clinician. J Psychiatr Res 12:189–198.

Frasch MG, Walter B, Friedrich H, Hoyer D, Eiselt M, Bauer R (2007): Detecting the signature of reticulothalamocortical communication in cerebrocortical electrical activity. Clin Neurophysiol 118:1969–1979.

Friston K, Ashburner J, Frith CD, Poline J-B, Heather JD, Frackowiak RSJ (1995a): Spatial registration and normalization of image. Hum Brain Mapp 2:165–189.

Friston K, Holmes AP, Worsley K, Poline J-B, Frith CD, Frackowiak RSJ (1995b): Statistical parametric maps in functional imaging: A general linear approach. Hum Brain Mapp 2:189–210.

Friston KJ, Poline J-B, Holmes AP, Frith CD, Frackowiak RSJ (1996): A multivariate analysis of PET activation studies. Hum Brain Map 4:140–151.

Giannakopoulos P, Hof PR, Michel JP, Guimon J, Bouras C (1997): Cerebral cortex pathology in aging and Alzheimer's disease: A quantitative survey of large hospital-based geriatric and psychiatric cohorts. Brain Res Brain Res Rev 25:217–245.

Greicius MD, Srivastava G, Reiss AL, Menon V (2004): Default-mode network activity distinguishes Alzheimer's disease from healthy aging: Evidence from functional MRI. Proc Natl Acad Sci USA 101:4637–4642.

Hampel H, Teipel SJ, Alexander GE, Pogarell O, Rapoport SI, Moller HJ (2002): In vivo imaging of region and cell type specific neocortical neurodegeneration in Alzheimer's disease perspectives of MRI derived corpus callosum measurement for mapping disease progression and effects of therapy. Evidence from studies with MRI, EEG and PET. J Neural Transm 109:837–855.

Head D, Buckner RL, Shimony JS, Williams LE, Akbudak E, Conturo TE, McAvoy M, Morris JC, Snyder AZ (2004): Differential vulnerability of anterior white matter in nondemented aging with minimal acceleration in dementia of the Alzheimer type: Evidence from diffusion tensor imaging. Cereb Cortex 14:410–423.

Huang J, Auchus AP (2007): Diffusion tensor imaging of normal appearing white matter and its correlation with cognitive functioning in mild cognitive impairment and Alzheimer's disease. Ann NY Acad Sci 1097, 259–264.

Jelic V, Johansson SE, Almkvist O, Shigeta M, Julin P, Nordberg A, Winblad B, Wahlund LO (2000): Quantitative electroencephalography in mild cognitive impairment: Longitudinal changes and possible prediction of Alzheimer's disease. Neurobiol Aging 21:533–540.

Jelic V, Shigeta M, Julin P, Almkvist O, Winblad B, Wahlund LO (1996): Quantitative electroencephalography power and coherence in Alzheimer's disease and mild cognitive impairment. Dementia 7:314–323.

Jiang ZY, Zheng LL (2006): Inter- and intra-hemispheric EEG coherence in patients with mild cognitive impairment at rest and during working memory task. J Zhejiang Univ Sci B 7:357–364.

Klimesch W (1997): EEG-α rhythms and memory processes. Int J Psychophysiol 26:319–340.

Klimesch W, Schack B, Sauseng P (2005): The functional significance of theta and upper α oscillations. Exp Psychol 52:99–108.

Koenig T, Prichep L, Dierks T, Hubl D, Wahlund LO, John ER, Jelic V (2005): Decreased EEG synchronization in Alzheimer's disease and mild cognitive impairment. Neurobiol Aging 26:165–171.

Kowall NW, Kosik KS (1987): Axonal disruption and aberrant localization of tau protein characterize the neuropil pathology of Alzheimer's disease. Ann Neurol 22:639–643.

Laufs H, Kleinschmidt A, Beyerle A, Eger E, Salek-Haddadi A, Preibisch C, Krakow K (2003a): EEG-correlated fMRI of human α activity. Neuroimage 19:1463–1476.

Laufs H, Krakow K, Sterzer P, Eger E, Beyerle A, Salek-Haddadi A, Kleinschmidt A (2003b): Electroencephalographic signatures of attentional and cognitive default modes in spontaneous brain activity fluctuations at rest. Proc Natl Acad Sci USA 100:11053–11058.

Leocani L, Locatelli T, Martinelli V, Rovaris M, Falautano M, Filippi M, Magnani G, Comi G (2000): Electroencephalographic coherence analysis in multiple sclerosis: Correlation with clinical, neuropsychological, and MRI findings. J Neurol Neurosurg Psychiatry 69:192–198.

Leys D, Pruvo JP, Parent M, Vermersch P, Soetaert G, Steinling M, Delacourte A, Defossez A, Rapoport A, Clarisse J (1991): Could Wallerian degeneration contribute to ''leuko-araiosis'' in subjects free of any vascular disorder? J Neurol Neurosurg Psychiatry 54:46–50.

Maioli F, Coveri M, Pagni P, Chiandetti C, Marchetti C, Ciarrocchi R, Ruggero C, Nativio V, Onesti A, D'Anastasio C, Pedone V (2007): Conversion of mild cognitive impairment to dementia in elderly subjects: A preliminary study in a memory and cognitive disorder unit. Arch Gerontol Geriatr 44 (Suppl 1):233–241.

Mangin JF, Poupon C, Clark C, Le Bihan D, Bloch I (2002): Distortion correction and robust tensor estimation for MR diffusion imaging. Med Image Anal 6:191–198.

Marosi E, Harmony T, Sanchez L, Becker J, Bernal J, Reyes A, Diaz de Leon AE, Rodriguez M, Fernandez T (1992): Maturation of the coherence of EEG activity in normal and learning-disabled children. Electroencephalogr Clin Neurophysiol 83:350–357.

Medina D, Detoledo-Morrell L, Urresta F, Gabrieli JD, Moseley M, Fleischman D, Bennett DA, Leurgans S, Turner DA, Stebbins GT (2006): White matter changes in mild cognitive impairment and AD: A diffusion tensor imaging study. Neurobiol Aging 27:663–672.

Miller R (2007): Theory of the normal waking EEG: From single neurones to waveforms in the α, β and γ frequency ranges. Int J Psychophysiol 64:18–23.

Montplaisir J, Nielsen T, Cote J, Boivin D, Rouleau I, Lapierre G (1990): Interhemispheric EEG coherence before and after partial callosotomy. Clin Electroencephalogr 21:42–47.

Morgane PJ, Bronzino JD, Kennard MM (1981): PGO wave activity and cortical EEG in the reserpinized, anesthetized cat. Sleep 4:207–219.

Morrison JH, Scherr S, Lewis DA, Campbell MJ, Bloom FE (1986): The laminar and regional distribution of neocortical somatostatin and neuritic plaques: Implications for Alzheimer's disease as a global neocortical disconnection syndrome. In: Scheibel AB, Weschler AF, editors. The Biological Substrates of Alzheimer's Disease, New York: Academic Press. pp 115–131.

Müller MJ, Greverus D, Dellani PR, Weibrich C, Wille PR, Scheurich A, Stoeter P, Fellgiebel A (2005): Functional implications of hippocampal volume and diffusivity in mild cognitive impairment. Neuroimage 28:1033–1042.

Muller MJ, Greverus D, Weibrich C, Dellani PR, Scheurich A, Stoeter P, Fellgiebel A (2007): Diagnostic utility of hippocampal size and mean diffusivity in amnestic MCI. Neurobiol Aging 28:398–403.

Naggara O, Oppenheim C, Rieu D, Raoux N, Rodrigo S, Dalla Barba G, Meder JF (2006): Diffusion tensor imaging in early Alzheimer's disease. Psychiatry Res 146:243–249.

Newton TF, Leuchter AF, Walter DO, Van Gorp WC, Stern CE, Mandelkern M, Weiner H (1993): EEG coherence in men with AIDS: Association with subcortical metabolic activity. J Neuropsychiatry Clin Neurosci 5:316–321.

Nunez PL, Srinivasan R, Westdorp AF, Wijesinghe RS, Tucker DM, Silberstein RB, Cadusch PJ (1997): EEG coherency. I. Statistics, reference electrode, volume conduction, Laplacians, cortical imaging, and interpretation at multiple scales. Electroencephalogr Clin Neurophysiol 103:499–515.

Nunez PL, Silberstein RB, Shi Z, Carpenter MR, Srinivasan R, Tucker DM, Doran SM, Cadusch PJ, Wijesinghe RS (1999): EEG coherency. II. Experimental comparisons of multiple measures. Clin Neurophysiol 110:469–486.

Nunez PL, Wingeier BM, Silberstein RB (2001): Spatial-temporal structures of human α rhythms: Theory, microcurrent sources, multiscale measurements, and global binding of local networks. Hum Brain Mapp 13:125–164.

Nuwer MR, Comi G, Emerson R, Fuglsang-Frederiksen A, Guerit JM, Hinrichs H, Ikeda A, Luccas FJ, Rappelsburger P (1998): IFCN standards for digital recording of clinical EEG. International Federation of Clinical Neurophysiology. Electroencephalogr Clin Neurophysiol 106:259–261.

Pandya DN, Seltzer B (1986): The topography of commissural fibres. In: Lepre F, Ptito M,Jasper HH, editors. Two Hemispheres—One Brain: Functions of the Corpus Callosum. New York: Alan R Liss. pp 47–73.

Pearson RCA, Esiri MM, Hiorns RW, Wilcock GK, Powell TPS (1985): Anatomical correlates of the distribution of the pathological changes in the neocortex in Alzheimer's disease. Proc Natl Acad Sci USA 82:4531–4534.

Petersen RC (2004): Mild cognitive impairment as a diagnostic entity. J Intern Med 256:183–194.

Petersen RC, Smith GE, Waring SC, Ivnik RJ, Tangalos EG, Kokmen E (1999): Mild cognitive impairment: Clinical characterization and outcome. Arch Neurol 56:303–308.

Petersen RC, Doody R, Kurz A, Mohs RC, Morris JC, Rabins PV, Ritchie K, Rossor M, Thal L, Winblad B (2001): Current concepts in mild cognitive impairment. Arch Neurol 58:1985–1992.

Pogarell O, Teipel SJ, Juckel G, Gootjes L, Moller T, Burger K, Leinsinger G, Moller HJ, Hegerl U, Hampel H (2005): EEG coherence reflects regional corpus callosum area in Alzheimer's disease. J Neurol Neurosurg Psychiatry 76:109–111.

Prichep LS (2007): Quantitative EEG and electromagnetic brain imaging in aging and in the evolution of dementia. Ann NY Acad Sci 1097:156–167.

Robinson PA (2003): Neurophysical theory of coherence and correlations of electroencephalographic and electrocorticographic signals. J Theor Biol 222:163–175.

Robinson PA, Rennie CJ, Rowe DL, O'Connor SC, Wright JJ, Gordon E, Whitehouse RW (2003): Neurophysical modeling of brain dynamics. Neuropsychopharmacology 28 (Suppl 1):S74–S79.

Rose SE, Chen F, Chalk JB, Zelaya FO, Strugnell WE, Benson M, Semple J, Doddrell DM (2000): Loss of connectivity in Alzheimer's disease: An evaluation of white matter tract integrity with colour coded MR diffusion tensor imaging. J Neurol Neurosurg Psychiatry 69:528–530.

Rose SE, McMahon KL, Janke AL, O'Dowd B, de Zubicaray G, Strudwick MW, Chalk JB (2006): Diffusion indices on magnetic resonance imaging and neuropsychological performance in amnestic mild cognitive impairment. J Neurol Neurosurg Psychiatry 77:1122–1128.

Rossini PM, Del Percio C, Pasqualetti P, Cassetta E, Binetti G, Dal Forno G, Ferreri F, Frisoni G, Chiovenda P, Miniussi C, Parisi L, Tombini M, Vecchio F, Babiloni C (2006): Conversion from mild cognitive impairment to Alzheimer's disease is predicted by sources and coherence of brain electroencephalography rhythms. Neuroscience 143:793–803.

Rossini PM, Buscema M, Capriotti M, Grossi E, Rodriguez G, Del Percio C, Babiloni C (2008): Is it possible to automatically distinguish resting EEG data of normal elderly vs. mild cognitive impairment subjects with high degree of accuracy? Clin Neurophysiol 119:1534–1545.

Saltzberg B, Burton WD Jr, Burch NR, Fletcher J, Michaels R (1986): Electrophysiological measures of regional neural interactive coupling. Linear and non-linear dependence relationships among multiple channel electroencephalographic recordings. Int J Biomed Comput 18:77–87.

Sarnthein J, Jeanmonod D (2007): High thalamocortical theta coherence in patients with Parkinson's disease. J Neurosci 27:124–131.

Schaltenbrand G, Spuler H, Wahren W (1970): Electroanatomy of the corpus callosum radiation according to the facts of stereotactic stimulation in man. Z Neurol 198:79–92.

Scheltens P, Barkhof F, Leys D, Pruvo JP, Nauta JJP, Vermersch P, Steinling M, Valk J (1993): A semiquantitative rating scale for the assessment of signal hyperintensities on magnetic resonance imaging. J Neurol Sci 114:7–12.

Schmid RG, Tirsch WS, Rappelsberger P, Weinmann HM, Poppl SJ (1992): Comparative coherence studies in healthy volunteers and Down's syndrome patients from childhood to adult age. Electroencephalogr Clin Neurophysiol 83:112–123.

Shulman KI, Shedletsky R, Silver IL (1986): The challenge of time: Clock drawing and cognitive function in the elderly. Int J Geriatr Psychiatry 1:135–140.

Sillito AM, Jones HE, Gerstein GL, West DC (1994): Feature-linked synchronization of thalamic relay cell firing induced by feedback from the visual cortex. Nature 369:479–482.

Silverman D (1960): The anterior temporal electrode and the ten-twenty system. Electroencephalogr Clin Neurophysiol 12:735–737.

Soteropoulos DS, Baker SN (2006): Cortico-cerebellar coherence during a precision grip task in the monkey. J Neurophysiol 95:1194–1206.

Sporns O, Chialvo DR, Kaiser M, Hilgetag CC (2004): Organization, development and function of complex brain networks. Trends Cogn Sci 8:418–425.

Stahl R, Dietrich O, Teipel SJ, Hampel H, Reiser MF, Schoenberg SO (2007): White matter damage in Alzheimer's disease and in mild cognitive impairment: Assessment with diffusion tensor MRI using parallel imaging techniques. Radiology 243:483–492.

Stam CJ, Hessels-van der Leij EM, Meulstee J, Vliegen JH (2000): Changes in functional coupling between neural networks in the brain during maturation revealed by omega complexity. Clin Electroencephalogr 31:104–108.

Steriade M (1995): Brain activation, then (1949) and now: Coherent fast rhythms in corticothalamic networks. Arch Ital Biol 134: 5–20.

Su JH, Cummings BJ, Cotman CW (1993): Identification and distribution of axonal dystrophic neurites in Alzheimer's disease. Brain Res 625:228–237.

Sudmeyer M, Pollok B, Hefter H, Gross J, Butz M, Wojtecki L, Timmermann L, Schnitzler A (2006): Synchronized brain network underlying postural tremor in Wilson's disease. Mov Disord 21:1935–1940.

Takahashi S, Yonezawa H, Takahashi J, Kudo M, Inoue T, Tohgi H (2002): Selective reduction of diffusion anisotropy in white matter of Alzheimer disease brains measured by 3.0 Tesla magnetic resonance imaging. Neurosci Lett 332:45–48.

Talairach J, Tournoux P (1988): Co-Planar Stereotaxic Atlas of the Human Brain. New York: Thieme.

Tao HY, Tian X (2005): Coherence characteristics of γ-band EEG during rest and cognitive task in MCI and AD. Conf Proc IEEE Eng Med Biol Soc 3:2747–2750.

Teipel SJ, Stahl R, Dietrich O, Schoenberg SO, Perneczky R, Bokde AL, Reiser MF, Moller HJ, Hampel H (2007): Multivariate network analysis of fiber tract integrity in Alzheimer's disease. Neuroimage 34:985–995.

Thatcher RW (1992): Cyclic cortical reorganization during early childhood. Brain Cogn 20:24–50.

Thatcher RW, Krause PJ, Hrybyk M (1986): Cortico-cortical associations and EEG coherence: A two-compartmental model. Electroencephalogr Clin Neurophysiol 64:123–143.

Thatcher RW, North DM, Biver CJ (2007): Development of cortical connections as measured by EEG coherence and phase delays. Hum Brain Mapp; Epub ahead of print.

Walter DO (1968): Coherence as a measure of relationship between EEG records. Electroencephalogr Clin Neurophysiol 24:282.

Wang G, Takigawa M, Matsushita T (1992): Correlation of α activity between the frontal and occipital cortex. Jpn J Physiol 42:1–13.

Yoshiura T, Mihara F, Ogomori K, Tanaka A, Kaneko K, Masuda K (2002): Diffusion tensor in posterior cingulate gyrus: Correlation with cognitive decline in Alzheimer's disease. Neuroreport 13:2299–2302.

Zhang Y, Schuff N, Jahng GH, Bayne W, Mori S, Schad L, Mueller S, Du AT, Kramer JH, Yaffe K, Chui H, Jagust WJ, Miller BL, Weiner MW (2007): Diffusion tensor imaging of cingulum fibers in mild cognitive impairment and Alzheimer disease. Neurology 68:13–19.